Field Implementation of Fiber-Reinforced Polymer (FRP) Bridge Deck Panels

Prepared by:
Jeffery S. Volz, SE, PE, PhD (Principal Investigator)
Kamal H. Khayat, PhD, P.Eng. (Co-Principal Investigator)
Soo Duck Hwang
Hesham Tuwair
Jonathan T. Drury
Amy S. Crone
University of Oklahoma

FINAL Report

TR201516

Field Implementation of Fiber-Reinforced Polymer (FRP) Bridge Deck Panels

By

Jeffery S. Volz, SE, PE, PhD (Principal Investigator)
Kamal H. Khayat (Co-Principal Investigator)
Soo Duck Hwang
Hesham Tuwair
Jonathan T. Drury
Amy S. Crone

University of Oklahoma, Norman, Oklahoma

September 2016

TECHNICAL REPORT DOCUMENTATION PAGE

1. Report No. cmr 17-008	2. Government Accession No.	3. Recipient's Catalog No.
4. Title and Subtitle Field Implementation of Fiber-Reinforced Polymer (FRP) Deck Panels		**5. Report Date** September 2016 Published: June 2017
		6. Performing Organization Code 105 3477 00
7. Author(s) Jeffery S. Volz, S.E., P.E., Ph.D., Kamal H. Khayat, PhD, P.Eng. http://orcid.org/0000-0003-1431-0715, Soo Duck Hwang, Ph.D. http://orcid.org/0000-0003-2178-1531, Hesham Tuwair, Ph.D., Jonathan T. Drury, Amy S. Crone		**8. Performing Organization Report No.** Final Report 105 3477 00
9. Performing Organization Name and Address University of Oklahoma School of Civil Engineering and Environmental Science 202 W. Boyd St., Norman, OK 73019		**10. Work Unit No.**
		11. Contract or Grant No. MoDOT project # TR201516
12. Sponsoring Agency Name and Address Missouri Department of Transportation (SPR) Construction and Materials Division P.O. Box 270, Jefferson City, MO 65102		**13. Type of Report and Period Covered** Final Report (October 20, 2014 to October 15, 2016)
		14. Sponsoring Agency Code

15. Supplementary Notes

Conducted in cooperation with the U.S. Department of Transportation, Federal Highway Administration. MoDOT research reports are available in the Innovation Library at http://www.modot.org/services/or/byDate.htm. This report is available at https://library.modot.mo.gov/RDT/reports/TR201516/

16. Abstract

Although still in their infancy, fiber-reinforced polymer (FRP) bridges have shown great promise in eliminating corrosion concerns and meeting (or exceeding) FHWA's goal of 100-year life spans for bridges. While FRP bridges are cost-effective in terms of life cycle analyses, the combination of higher first costs and limited state DOT budgets has restricted their use. This research study examined a prototype FRP deck panel that incorporated polyurethane foam in an attempt to reduce the initial costs. The objective of this research was to develop the design methodology and construction details necessary to implement the prototype FRP deck panel on an actual bridge, addressing issues such as panel-to-panel connections, panel-to-girder connections, bridge skew, roadway crown, overlay materials, bridge guardrail attachment, and deck drainage. The full scale, prototype FRP deck panels performed exceptionally during all phases of testing. In general, results of the study indicated that the panels significantly exceeded the code required design forces in all instances. In flexure, shear and bearing, the average failure load exceeded the AASHTO Design Truck factored wheel load by nearly three times. Even more importantly, the panels behaved linearly-elastically throughout the full range of loading and possessed significant post-buckling strength. In terms of construction details, the panel-to-panel connection indicated 100% load transfer up to a load of over twice the AASHTO Design Truck factored wheel load and, in fact, the panel failed due to localized bearing prior to any failure of the joint. Furthermore, testing of the guardrail-to-panel connection for the prototype FRP deck panels indicated that without any modifications, the panels satisfy the AASHTO TL-2 guardrail requirements. To attain an AASHTO TL-3 or TL-4 level, the panels would require localized reinforcement at the guardrail post connection points. In terms of potential overlay materials, epoxy-based polymer concretes offered the greatest bond strengths and thermal compatibility with the FRP deck. Finally, it appears that existing FRP design equations can reasonably predict the response and behavior of the VARTM-manufactured, prototype FRP bridge deck panels. The equations correctly predicted a flexural failure due to local buckling of the compression flange and a bearing failure due to local buckling of the webs beneath the concentrated load.

17. Key Words	18. Distribution Statement
Anchors (Structural connectors); Benefit cost analysis; Bridge decks; Fiber reinforced polymers; Field tests; Guardrails; Implementation. Concrete; Concrete pavements; Paving; Recycled materials; Sustainable development	No restrictions. This document is available through the National Technical Information Service, Springfield, VA 22161.

19. Security Classif. (of this report) Unclassified.	20. Security Classif. (of this page) Unclassified.	21. No. of Pages 85	22. Price

Form DOT F 1700.7 (8-72)   Reproduction of completed page authorized

EXECUTIVE SUMMARY

On behalf of the Missouri Department of Transportation (MoDOT), the University of Oklahoma and Missouri University of Science and Technology completed a research study on a novel fiber-reinforced polymer (FRP) bridge deck panel that incorporates polyurethane foam infill. The objective of the research was to develop the design methodology and construction details necessary to implement the FRP deck panels on an actual bridge, addressing issues such as panel-to-panel connections, panel-to-girder connections, bridge skew, roadway crown, overlay materials, bridge guardrail attachment, and deck drainage. This report documents the results of this study.

The report is composed of eight chapters. Chapter 1 gives a brief introduction to the subject area, explains the necessity of this research, and also presents the objectives and scope of work of the investigation. Chapter 2 explains the fabrication process to construct the full scale, prototype FRP deck panels. Chapter 3 presents the full scale panel testing necessary to verify the performance and behavior of a large sample of industrially-manufactured deck panels as well as calibrate existing design equations for the VARTM manufacturing process. Chapter 4 details the testing and evaluation of alternative panel-to-panel connection details for the prototype FRP deck panels. Chapter 5 presents the testing and evaluation of the guardrail-to-panel connection for the deck panels. Chapter 6 evaluates the applicability of existing FRP design equations when used for the design of the VARTM-manufactured, prototype FRP bridge deck. Chapter 7 contains a detailed study of alternative overlay materials to both protect the top facesheets of the panels and to provide a wearing/traction surface for vehicular traffic. Finally, Chapter 8 presents additional design issues necessary to implement the prototype FRP deck panels on an actual bridge.

The full scale, prototype FRP deck panels performed exceptionally during all phases of testing. In general, results of the study indicated that the panels significantly exceeded the code required design forces in all instances. In flexure, shear and bearing, the average failure load exceeded the AASHTO Design Truck factored wheel load by nearly three times. Even more importantly, the panels behaved linearly-elastically throughout the full range of loading and possessed significant post-buckling strength. In terms of construction details, the panel-to-panel connection indicated 100% load transfer up to a load of over twice the AASHTO Design Truck factored wheel load and, in fact, the panel failed due to localized bearing prior to any failure of the joint. Furthermore, testing of the guardrail-to-panel connection for the prototype FRP deck panels indicated that without any modifications, the panels satisfy the AASHTO TL-2 guardrail requirements. To attain an AASHTO TL-3 or TL-4 level, the panels would require localized reinforcement at the guardrail post connection points. In terms of potential overlay materials, epoxy-based polymer concretes offered the greatest bond strengths and thermal compatibility with the FRP deck. Finally, it appears that existing FRP design equations can reasonably predict the response and behavior of the VARTM-manufactured, prototype FRP bridge deck panels. The equations correctly predicted a flexural failure due to local buckling of the compression flange and a bearing failure due to local buckling of the webs beneath the concentrated load.

ACKNOWLEDGEMENTS

TABLE OF CONTENTS

Page

TABLE OF CONTENTS (cont'd)

LIST OF ILLUSTRATIONS

LIST OF ILLUSTRATIONS (cont'd)

LIST OF ILLUSTRATIONS (cont'd)

LIST OF TABLES

1. INTRODUCTION

In December of 2011, the Missouri Department of Transportation (MoDOT) funded a study to examine the potential of fiber-reinforced polymer (FRP) bridge decks for highway bridges. The objective of that study, which will be referred to as Phase I, was to develop, test, and evaluate fiber-reinforced, polyurethane (PU) foams to replace the costly honeycomb construction currently used to manufacture FRP bridge deck panels. Initially, the effort focused on developing an FRP sandwich panel to replace the precast, stay-in-place forms currently used to construct reinforced concrete bridge decks. However, during the course of the project, the research effort expanded to include full-depth bridge deck panels as well.

The results of Phase I included the development of a prototype PU-FRP deck configuration, shown in **Figure 1.1**. This multicellular trapezoidal section eliminates the typical honeycomb construction by utilizing the PU foam as a stay-in-place form. Although very light weight and relatively flexible, the PU foam also provides resistance to local buckling of the top and bottom facesheets and the sloping webs. The combination of the trapezoidal PU foam cores and FRP flanges and webs results in a very efficient cross section. This prototype deck configuration has an overall depth of 9-1/4 in. and is fabricated using the vacuum assisted resin transfer molding (VARTM) process.
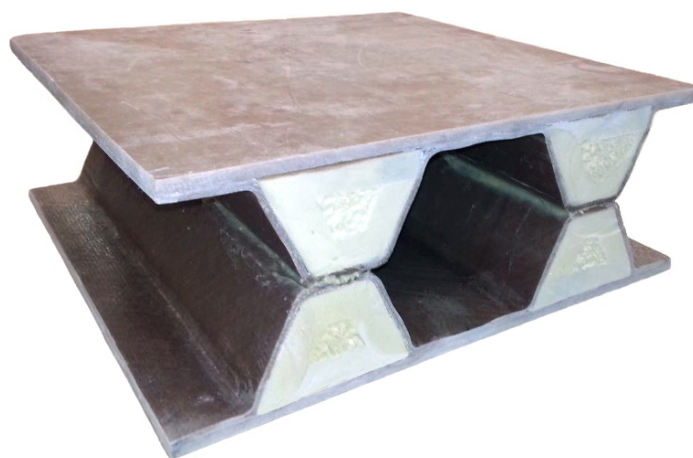
Figure 1.1: Prototype PU-FRP Deck Configuration

The prototype development focused on the feasibility of a PU-FRP deck configuration through a study of four different sandwich types: high density foam; low density foam with FRP webs; low density stitched foam; and trapezoidal, low-density foam with mat reinforcement. This study included component testing; small-scale sandwich panel flexural testing; mid-scale sandwich panel testing under static, fatigue, and environmental exposure; and analytical modeling of the prototype panel. The next phase, presented in this report and referred to as Phase II, focused on developing the design methodology and construction details necessary to

implement FRP deck panels on an actual bridge, addressing issues such as panel-to-panel connections, panel-to-girder connections, bridge skew, roadway crown, bridge guardrail attachment, and deck drainage.

1.1. PROBLEM STATEMENT AND JUSTIFICATION

The deterioration of our nation's infrastructure is an almost daily news item that attracts passionate political, economic, and socio-economic discussions. One of the leading causes of this deterioration is the "bare roads policy" adopted by the majority of state highway agencies during the 1960's. This policy involves the application of deicing salts on state roads during winter months to reduce traffic accidents, injuries, and fatalities. An unfortunate side effect of this policy is that deicing salts attack the steel embedded in reinforced concrete bridges, leading to premature deterioration. In 2002, a study sponsored by the Federal Highway Administration (Koch, et al., 2002) predicted that the U.S. will spend an estimated 8.3 billion dollars annually over the next twenty years in an effort to repair or replace bridges exhibiting corrosion-related damage, with indirect costs exceeding 10 times that amount.

Although still in their infancy, fiber-reinforced polymer (FRP) bridges have shown great promise in eliminating corrosion concerns and meeting (or exceeding) FHWA's goal of 100-year life spans for bridges. While FRP bridges are cost-effective in terms of life cycle analyses, the combination of higher first costs and limited state DOT budgets has restricted their use. One area that has shown some headway is the use of FRP for bridge decks, focusing on the location where the majority of corrosion-related damage normally occurs. However, first costs still hamper widespread use of this approach.

FRP bridge deck panels offer superior corrosion resistance, at one-fifth the weight of reinforced concrete. However, current FRP bridge deck panels typically rely on an intricate geometric honeycomb system between the top and bottom layers of the sandwich panel. This labor-intensive honeycomb construction doubles the cost of FRP panels compared to reinforced concrete. Although cost-effective in terms of longevity of the bridge and overall reductions in weight, the lower first cost of reinforced concrete precludes the use of FRP bridge decks in the majority of situations.

Closed-cell, high-density polyurethane foams lower first cost, offering a cost-effective alternative to the complex honeycomb construction. Structural sandwich panels with a polyurethane foam infill are well established in other commercial applications, such as automobiles, aircraft, and prefabricated buildings. Several recent advances in polyurethane foam formulations have resulted in a material that can resist the localized compressive stresses and fatigue loading beneath a truck wheel, making this type of sandwich panel construction a viable alternative for bridge decks. Once these panels can compete against reinforced concrete on a first-cost basis, their significantly longer life expectancies will save considerable money for MoDOT and the residents of Missouri.

1.2. OBJECTIVE AND RESEARCH PLAN

The *objective* of the Phase II research was to develop the design methodology and construction details necessary to implement FRP deck panels on an actual bridge, addressing issues such as panel-to-panel connections, panel-to-girder connections, bridge skew, roadway crown, overlay materials, bridge guardrail attachment, and deck drainage.

The *research plan* involved designing, manufacturing, testing, and evaluating full-scale FRP deck panels; assessing the applicability of existing FRP design equations; developing, manufacturing, testing, and evaluating alternative panel-to-panel, panel-to-girder, and guardrail-to-panel connection details; investigating skewed bridge deck layout options; developing, testing, and evaluating alternative overlay materials; and examining costs of the prototype FRP deck. This report documents the results of this study.

1.3. TECHNICAL REPORT ORGANIZATION

This report documents a research project on a prototype FRP bridge deck performed by the University of Oklahoma and Missouri University of Science and Technology on behalf of the Missouri Department of Transportation (MoDOT).

The report is composed of eight chapters. Chapter 1 gives a brief introduction to the subject area, explains the necessity of this research, and also presents the objectives and scope of work of the investigation. Chapter 2 explains the fabrication process to construct the full scale, prototype FRP deck panels. Chapter 3 presents the full scale panel testing necessary to verify the performance and behavior of a large sample of industrially-manufactured deck panels as well as calibrate existing design equations for the VARTM manufacturing process. Chapter 4 details the testing and evaluation of alternative panel-to-panel connection details for the prototype FRP deck panels. Chapter 5 presents the testing and evaluation of the guardrail-to-panel connection for the deck panels. Chapter 6 evaluates the applicability of existing FRP design equations when used for the design of the VARTM-manufactured, prototype FRP bridge deck. Chapter 7 contains a detailed study of alternative overlay materials to both protect the top facesheets of the panels and to provide a wearing/traction surface for vehicular traffic. Finally, Chapter 8 presents additional design issues necessary to implement the prototype FRP deck panels on an actual bridge.

2. FABRICATION PROCESS FOR PROTOTYPE FRP DECK PANELS

Three manufacturing methods are typically used to produce FRP profiles (sections) for structural engineering applications. These methods consist of pultrusion, open mold hand layup, and vacuum assisted resin transfer molding (Bank, 2006). In the pultrusion process, an automated production line pulls dry fibers through a resin impregnator (bath) followed by a heated, chrome-plated steel die. The FRP material cures as it passes through the die, after which the section is cut to the desired lengths. In the open mold hand layup process, the FRP shape is manufactured using a rigid mold and hand placing successive layers of fibers, usually in the form of mats or weaves. As each layer of fiber is laid down, rollers or sprayers apply resin. Once all layers and resin have been applied, the part is placed in an oven to cure. In the vacuum assisted resin transfer molding (VARTM) process, the FRP shape is also manufactured using a rigid mold and hand placing successive layers of fibers. However, no resin is applied. Once the fibers are in place, the part is enclosed within a special bag and a series of pumps apply a vacuum, which compresses the fibers tightly against the mold. Resin, applied through feed lines, is drawn through the part by virtue of the vacuum, resulting in wetout of the fibers.

Each methods has advantages and disadvantages. The pultrusion process provides very high quality sections with tight tolerances but has a very high initial cost, limited custom sizes, and an inability to incorporate special features (i.e., only provides a constant cross section). The open mold hand layup process provides custom sizes at a very low initial cost but requires highly skilled workers to maintain quality control. The VARTM process also provides custom sizes at a very low initial cost compared to pultrusion but is slightly more expensive than the open mold process. Quality of fabrication for a VARTM part is between pultrusion and open mold hand layup. In general, the VARTM process offers a balance between cost and quality and was the method chosen to manufacture the prototype FRP deck panels for testing and evaluation as part of this research effort.

FRP is formed by combining fiber reinforcement with a resin. For most applications, fiberglass is used to provide the fiber reinforcement. The most common type of fiberglass reinforcement is a woven fabric, formed by interlacing a series of fiberglass yarns. More recently, fiberglass manufacturers have developed stitch bonded fabrics that eliminate the crimping inherent in a woven fabric. The prototype FRP deck sections were fabricated with stitch bonded fabrics. **Figure 2.1** is a schematic of a generalized stitch bonded fiberglass fabric. Fibers can be placed in the longitudinal 0° direction, transverse 90° direction, +45° direction, and −45° direction. The fibers are underlain with a chopped strand mat fabric, which is a layer of random 3 to 4 inch long fibers. All the fibers are then stitched together to form the fabric. Depending on the application, some of the fibers shown in the schematic are not included. For instance, if the loads are predominantly in the longitudinal direction, the fabric will only contain longitudinal 0° direction fibers, a minimal amount of transverse 90° fibers, and the chopped strand mat. The fabric architecture can be tailored to the specific application.

A schematic representation of the prototype FRP deck fabrication process is shown in **Figures 2.2** through **2.6**. A trapezoidal section of polyurethane foam forms the core of the cross section, **Figure 2.2**. A series of these foam sections are arranged in rows at the desired spacing as

shown in **Figure 2.3**. The next step involves successive placement of layers of stitch bonded fiberglass fabric around the foam core, shown diagrammatically in **Figure 2.4**. For the prototype deck, the facesheet consists of 12 layers of E-glass fabric while the sloping webs use 4 layers of E-glass fabric. Details and properties of the fabric architecture of each reinforcement layer are provided in **Table 2.1** and correspond to the designations shown in **Figure 2.4** (Fabrics 1, 2, and 3). This fabric layout results in the facesheet having an equal number of fibers in the longitudinal and transverse directions while the webs consist of fibers oriented at +45°/−45° to the longitudinal axis. This layout corresponds to the anticipated stresses, longitudinal and transverse in the facesheet and diagonal in the webs.
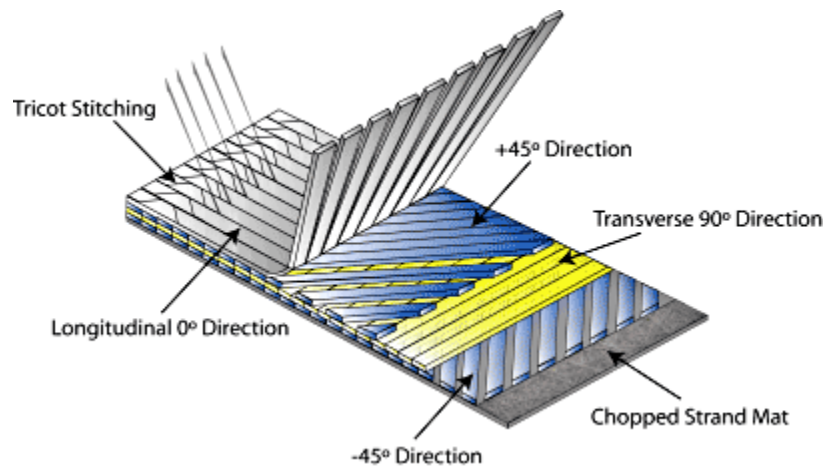
Figure 2.1: Generalized Schematic of Stitch Bonded Fiberglass Fabric (courtesy VectorPly Corporation)

Once all the reinforcement layers are in place, the cross section is covered with a layer of high permeability distribution media to facilitate resin flow followed by a peel ply layer to prevent adhesion to the vacuum bag. The entire section is then enclosed within the vacuum bag, and the resin is infused into the fiberglass layers through the VARTM process. The prototype deck used a newly formulated, two-part, thermoset, polyurethane resin developed by Bayer MaterialScience. This resin was also used to fabricate the FRP panels for Phase I of this research. The new resin has improved mechanical properties compared to commonly used polyester and vinyl ester resin systems. Although polyurethane resins have been used in the past, this new resin system has a longer pot life (working life), allowing applications involving complex and relatively large-scale pieces. The section is post-cured for 1 hour at 160°F then 4 hours at 180°F. The result of this process is the completed half panel segment shown in **Figure 2.5**. Two completed half panel segments are then bonded together with a methacrylate adhesive to form the overall deck section, **Figure 2.6**. Dimensions of the finished prototype deck panel are provided in **Figure 2.7**. The panel can be manufactured to any desired width and length.
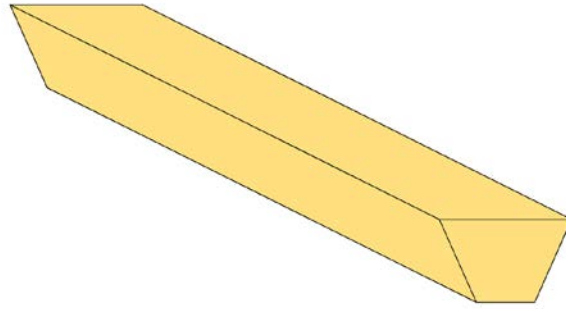
Figure 2.2: Trapezoidal-Shaped Polyurethane Foam Core
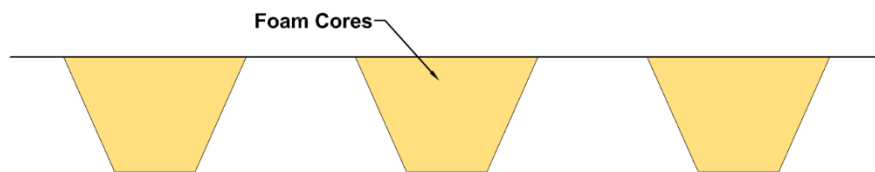
Figure 2.3: Foam Core Arrangement in Preparation for Fiberglass
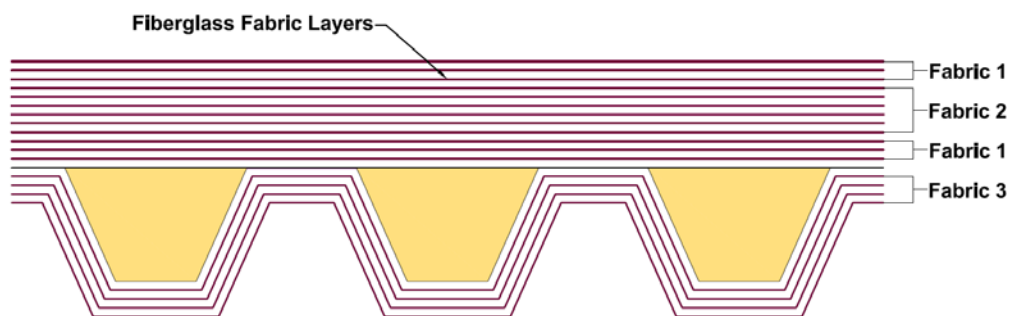
Figure 2.4: Placement of Layers of Fiberglass Fabric Around Core
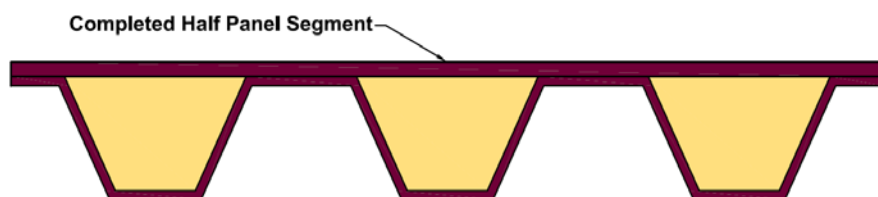
Figure 2.5: Completed Half Panel Segment
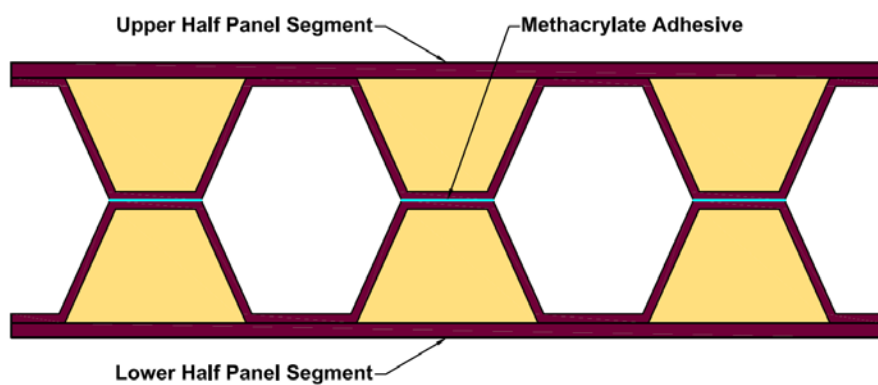
Figure 2.6: Overall Deck Section Formed by Bonding Two Half Panel Segments
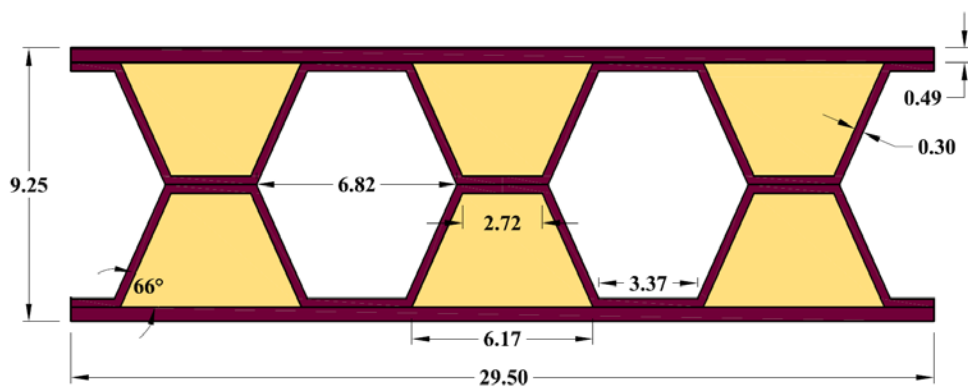
Figure 2.7: Dimensions of Finished Prototype Deck Panel
(Note: all dimensions in inches)

Table 2.1: Fiberglass Fabric Architecture and Properties

Property	Fabric 1 E-LM 1810 (90°)	Fabric 2 E-LM 1810 (0°)	Fabric 3 E-BXM 1715 (+45°/−45°)
0° Fiberglass	0.14 oz/yd^2	17.92 oz/yd^2	-
+45° Fiberglass	-	-	9.07 oz/yd^2
90° Fiberglass	17.92 oz/yd^2	0.14 oz/yd^2	-
−45° Fiberglass	-	-	9.07 oz/yd^2
Mat Fiberglass	9.00 oz/yd^2	9.00 oz/yd^2	8.10 oz/yd^2
Longitudinal Modulus (0°)	1,640 ksi	3,870 ksi	2,830 ksi
Transverse Modulus (90°)	3,870 ksi	1,640 ksi	2,830 ksi
Shear Modulus (+45°/−45°)	720 ksi	720 ksi	590 ksi
Longitudinal Tensile Strength (0°)	26.8 ksi	63.5 ksi	46.5 ksi
Longitudinal Compressive Strength (0°)	31.0 ksi	73.3 ksi	64.6 ksi
Transverse Tensile Strength (90°)	63.5 ksi	26.8 ksi	46.5 ksi
Transverse Compressive Strength (90°)	73.3 ksi	31.0 ksi	64.6 ksi
In-Plane Shear Strength (+45°/−45°)	16.3 ksi	16.3 ksi	13.4 ksi

3. FULL SCALE PROTOTYPE DECK PANEL TESTING

The next task of the research study involved manufacturing, testing, and evaluating full scale, prototype FRP deck panels. This step was necessary to verify the performance and behavior of a large sample of industrially-manufactured deck panels as well as calibrate existing design equations for the VARTM manufacturing process. The following section discusses the specimen fabrication and characteristics, details of the test setups and loading protocols, and the response and behavior of the specimens under various loading scenarios.

In Phase I, several alternative FRP deck configurations were developed, tested, and evaluated. Referred to as Type 1 (PU RIGID), Type 2 (WEB-CORE), and Type 3 (PRISMA FOAM), Type 3 was chosen to move forward to the prototype development stage. Phase I included testing of one section of full scale Type 3 deck. However, additional testing as part of Phase II is required to confirm the consistent response and behavior of this prototype section.

This series of full scale tests were also necessary to develop the design methodology for the prototype FRP deck panel. The VARTM process, discussed in detail in Section 2, is common in the automobile, marine, and industrial sectors. However, the design methodology for VARTM-constructed parts has not been quantified for transportation applications within civil engineering. The results of these full scale tests were used to verify the applicability of existing FRP design equations when used for the design of a VARTM-manufactured bridge deck.

3.1. TEST PANEL FABRICATION

The research team has been working with Structural Composites, Inc. – a composites manufacturing company located in West Melbourne, Florida – to transition the technology from the laboratory to an industrial manufacturing process. Structural Composites is the manufacturer of the polyurethane foam (PRISMA FOAM) used in Phase I of the research and which serves as the core of the prototype deck panel. They also manufacture a variety of composites for the automobile, trucking, and marine industries.

Working with Structural Composites and following the fabrication procedure discussed in detail in Section 2, the research team manufactured six (6) full-scale, prototype FRP deck sections for flexural, shear, and bearing stress testing. The deck panels had the following characteristics:

- Depth: 9¼"
- Width: 2'–5½"
- Length: 9'–9½"
- Span Length: 9'–2"

This panel width was chosen to represent the minimum panel width that would be expected on an actual bridge layout and thus the smallest section size that would be required to support the axle load of an AASHTO Design Truck (AASHTO LRFD, 2014). The panel length was chosen to represent a typical bridge girder spacing, although that dimension is less critical. The panel width determines the effective section able to support a concentrated wheel load assuming no load

transfer between adjacent panels, a worst case scenario. The complete dimensions of the cross section for the full scale test specimens are shown in **Figure 3.1**.
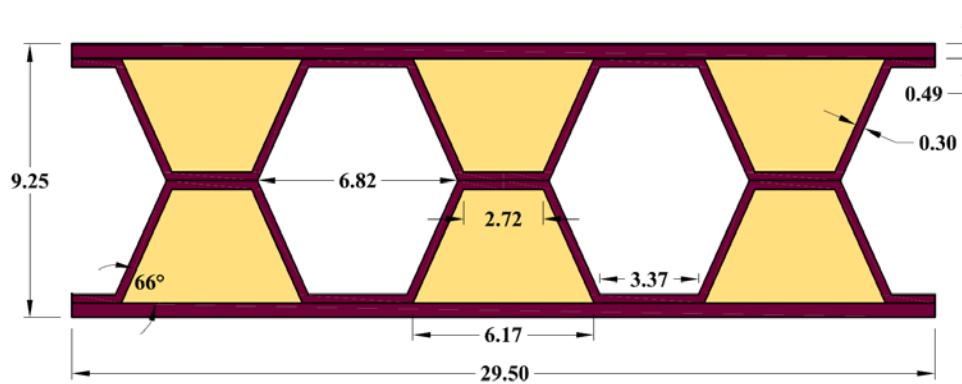
Figure 3.1: Full Scale Test Specimen Cross Section
(Note: all dimensions in inches)

3.2. FLEXURAL TEST SETUP AND LOADING PROTOCOL

A schematic of the flexural test setup is shown in **Figure 3.2**. The deck specimens are supported at each end by a concrete-filled steel tube to provide a roller support. A 1-in.-thick steel plate and 1/2-in.-thick rubber pad between the steel tube and deck specimens distributes the support reactions to prevent any stress concentrations. Concrete walls beneath the roller supports position the specimen at the required height within the load frame. Load is applied to the panel through a 300 kip Enerpac hydraulic ram and loading swivel. The loading swivel prevents stress concentrations as the panel deforms under load. A 200 kip load cell is positioned between the hydraulic ram and loading swivel to record the applied force. The applied force is distributed to the deck through a 2-in.-thick steel plate measuring 10 in. along the direction of traffic and 20 in. perpendicular to the direction of traffic in accordance with the AASHTO specified truck tire contact area (AASHTO LRFD, 2014). A 1-in.-thick neoprene pad placed between the steel plate and the deck surface mimics the rubber tires of a truck and also prevents any stress concentrations at the loading point. The loading point was positioned at midspan of the panel along the panel centerline in order to maximize the flexural stresses in the panel during the test.

Instrumentation for the flexural test specimens is shown in **Figure 3.3**. **Figure 3.3(a)** indicates the four spring potentiometers used to record the vertical deformation of the panel at midspan and the quarter point, with a series of potentiometers positioned along the panel centerline and a series positioned along the panel edge. Strain gages were installed along the top and bottom facesheets of the panels as shown in **Figures 3.3(b)** and **(c)**. A series of strain gauges were placed at midspan and the quarter point of the panels. Gauges S-1 through S-5 measured longitudinal strain and Gauge S-6 measured transverse strain of the top facesheet of the panel. Gauges S-7 through S-12 measured longitudinal strain and Gauges S-13 and S-14 measured

transverse strain of the bottom facesheet of the panel. All of the instrumentation was recorded through a data acquisition system.

A photograph of an FRP deck specimen within the test setup is shown in **Figure 3.4**.
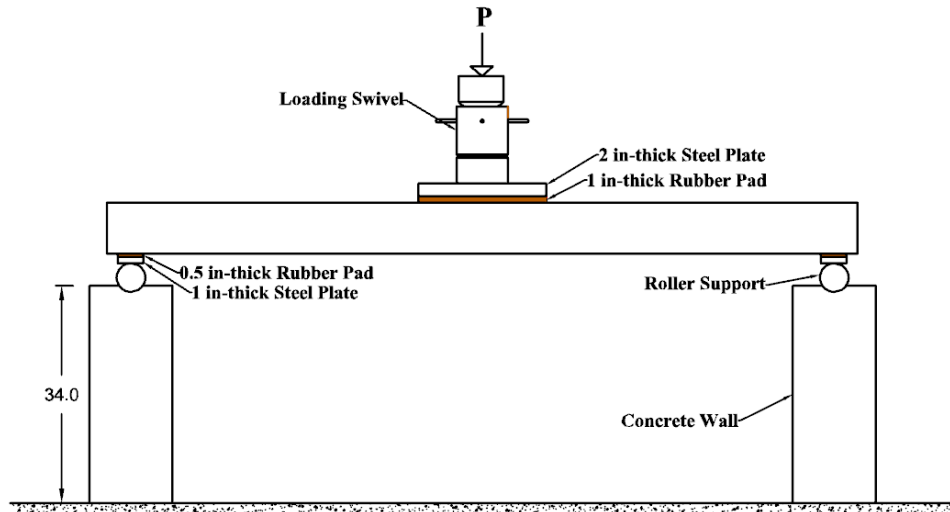
(a) Elevation View
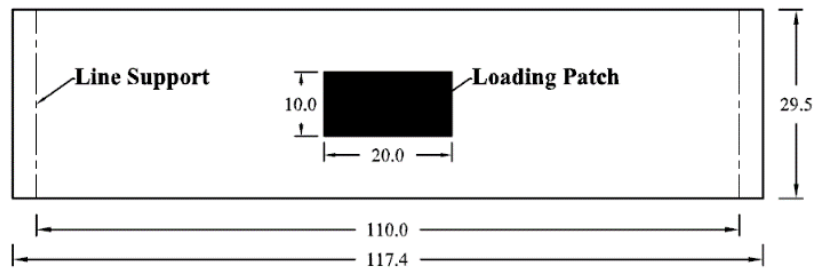
(b) Plan View

**Figure 3.2: Schematic of FRP Deck Flexural Test Setup
(Note: all dimensions in inches)**
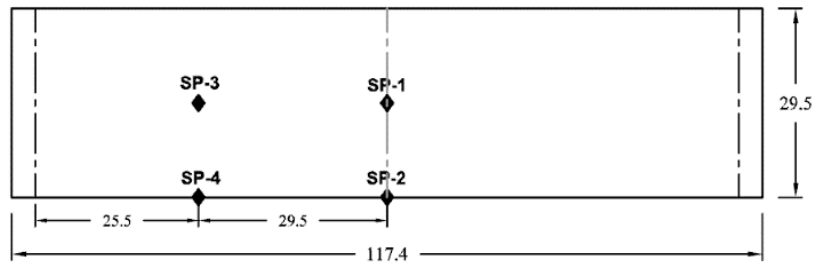
(a) Spring Potentiometer Layout
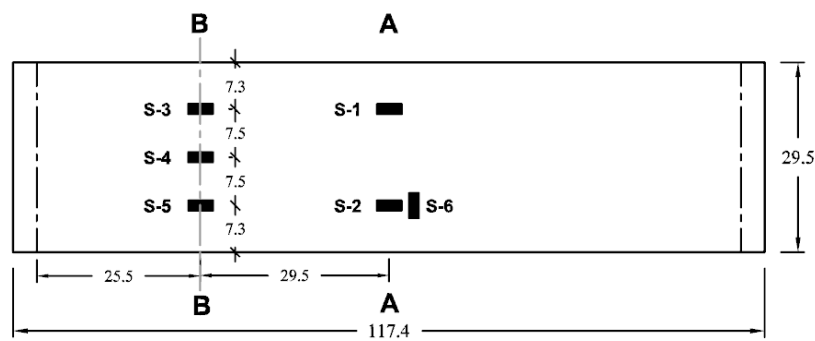
(b) Top Facesheet Strain Gauge Layout
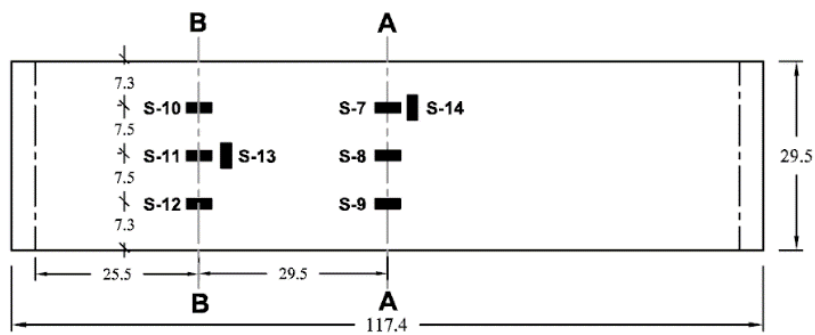
(c) Bottom Facesheet Strain Gauge Layout

**Figure 3.3: Instrumentation for FRP Deck Flexural Test Specimens
(Note: all dimensions in inches)**

Figure 3.4: Flexural Test Setup for FRP Deck Specimens

Loading protocol for the flexural test involved a progression of loading sequences based on the wheel load for an AASHTO Design Truck (AASHTO LRFD, 2014). The Design Truck wheel load equals 21.3 kips based on one half of the 32 kip axle load increased 33% for the dynamic load allowance. With the Strength I live load factor of 1.75, the full factored wheel load equals 37.2 kips. The loading sequences consisted of the following:

- Sequence No. 1: Load from zero to 21.3 kips (AASHTO Design Truck wheel load) then return to zero

- Sequence No. 2: Load from zero to 37.2 kips (AASHTO factored Design Truck wheel load) then return to zero

- Sequence No. 3: Load from zero to failure

The protocol consisted of three repetitions of Sequence No. 1, followed by three repetitions of Sequence No. 2, and then finished with testing the panel to failure, Sequence No. 3. At the end of each sequence, the panels were inspected for any signs of damage.

3.3. SHEAR AND BEARING TEST SETUP AND LOADING PROTOCOL

A schematic of the shear and bearing test setup is shown in **Figure 3.5**. The deck specimens are supported at each end by a concrete-filled steel tube to provide a roller support. A 1-in.-thick steel plate and 1/2-in.-thick rubber pad between the steel tube and deck specimens distributes the support reactions to prevent any stress concentrations. Concrete walls beneath the roller supports position the specimen at the required height within the load frame. Load is applied to the panel through a 300 kip Enerpac hydraulic ram and loading swivel. The loading swivel prevents stress concentrations as the panel deforms under load. A 200 kip load cell is

positioned between the hydraulic ram and loading swivel to record the applied force. The applied force is distributed to the deck through a 2-in.-thick steel plate measuring 10 in. along the direction of traffic and 20 in. perpendicular to the direction of traffic in accordance with the AASHTO specified truck tire contact area (AASHTO LRFD, 2014). A 1-in.-thick neoprene pad placed between the steel plate and the deck surface mimics the rubber tires of a truck and also prevents any stress concentrations at the loading point.

(a) Elevation View
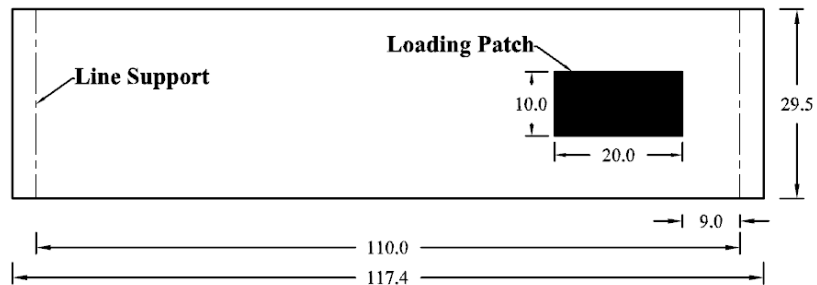
(b) Plan View

Figure 3.5: Schematic of FRP Deck Shear and Bearing Test Setup
(Note: all dimensions in inches)

The distance between the plate edge and the support was chosen to coincide with the overall panel depth, 9 in. This placement results in maximum shearing stresses coincident with the fiberglass orientation within the webs of the panels, which represents the typical behavior of the panel. A smaller distance between the loading point and support would result in a higher shear resistance of the panel due to engaging both the +45° and −45° fiberglass layers within the webs. In other words, a closer placement would provide a false reading and indicate a higher shear resistance of the panel than actually exists under loads placed farther from the support.

Instrumentation for the shear and bearing test specimens is shown in **Figure 3.6**. Unlike the flexural test specimens, no strain gauges were installed on the shear and bearing test specimens. Due to the physical characteristics of the panels, it was not possible to install strain gauges on the webs of the specimens. Therefore, only the four spring potentiometers were installed to record the vertical deformation of the panel at midspan and the quarter point, with a series of potentiometers positioned along the panel centerline and a series positioned along the panel edge. All of the instrumentation was recorded through a data acquisition system.

Loading protocol for the shear and bearing test involved loading the panel from zero to failure in increments of 5 kips. After each increment of load, the research team inspected the panel webs for any signs of damage.

A photograph of an FRP deck specimen within the test setup is shown in **Figure 3.7**.
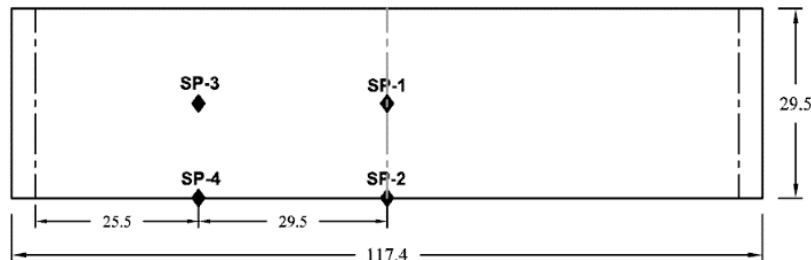
Figure 3.6: Instrumentation for FRP Deck Shear and Bearing Test Specimens (Note: all dimensions in inches)

3.4. RESULTS OF FLEXURAL TESTS

The research team tested three (3) full scale, prototype FRP deck panels in flexure following the test setup and loading protocol specified in Section 3.2. Overall, the panels were very consistent in terms of response and behavior. They all displayed a linear-elastic response throughout the full range of loading, and failure was initiated by local buckling of the compression flange (top facesheet) followed by separation of the flange from the webs along the panel length. This failure mode is typical for FRP structural members and is indicative of fully developing the cross section prior to any localized bearing failure beneath the concentrated load

point, which represents the point of application of the AASHTO Design Truck wheel load. A typical load-deflection plot for one of the FRP deck panels is shown in **Figure 3.8**, and a summary of the test results for the three (3) panels is provided in **Table 3.1**.

Figure 3.7: Shear and Bearing Test Setup for FRP Deck Specimens

The load-deflection plot of **Figure 3.8** reveals a number of important characteristics with regard to the response and behavior of the prototype FRP deck panels. First, as mentioned previously, the response is linear-elastic throughout the full range of loading. This behavior is typical for FRP material, but more importantly, the continued linear-elastic behavior during the full range of loading indicates no damage to the panel until reaching the peak load. Any intermediate damage would have resulted in a shift in the load-deflection response, which did not occur. Furthermore, no visible damage was observed during the different loading sequences within the testing protocol. The ability to withstand any damage until complete failure means that overloads experienced by the panels in service would not cause any permanent deformations or weakness in the bridge deck. These panels can support a load very near their failure point and return to their original shape once the load is removed.

Another important characteristic shown in the load-deflection plot is that the transverse stiffness of the panel helped to engage the majority of the cross section in supporting the applied point load. One issue with previous FRP deck systems was a lack of transverse stiffness to spread the truck tire wheel loads and engage as much of the cross section as possible. Transverse distribution of the concentrated wheel loads improves the efficiency and stiffness of the FRP deck system. In comparing gauges SP-1 and SP-2, there is only a 10% difference in the value of the centerline and edge deflection at midspan of the panel just prior to failure (2.103 in. vs. 1.883 in.). More importantly, at the service load level, 21.3 kips, there is only an 8% difference in deflection between the centerline and panel edge (0.411 in. vs. 0.378 in.). This relatively small

difference between the centerline and panel edge deformations indicates a small amount of transverse curvature of the panel and nearly full engagement of the cross section to support the concentrated wheel load. Similar behavior also occurred at the panel quarter point, gauges SP-3 and SP-4.
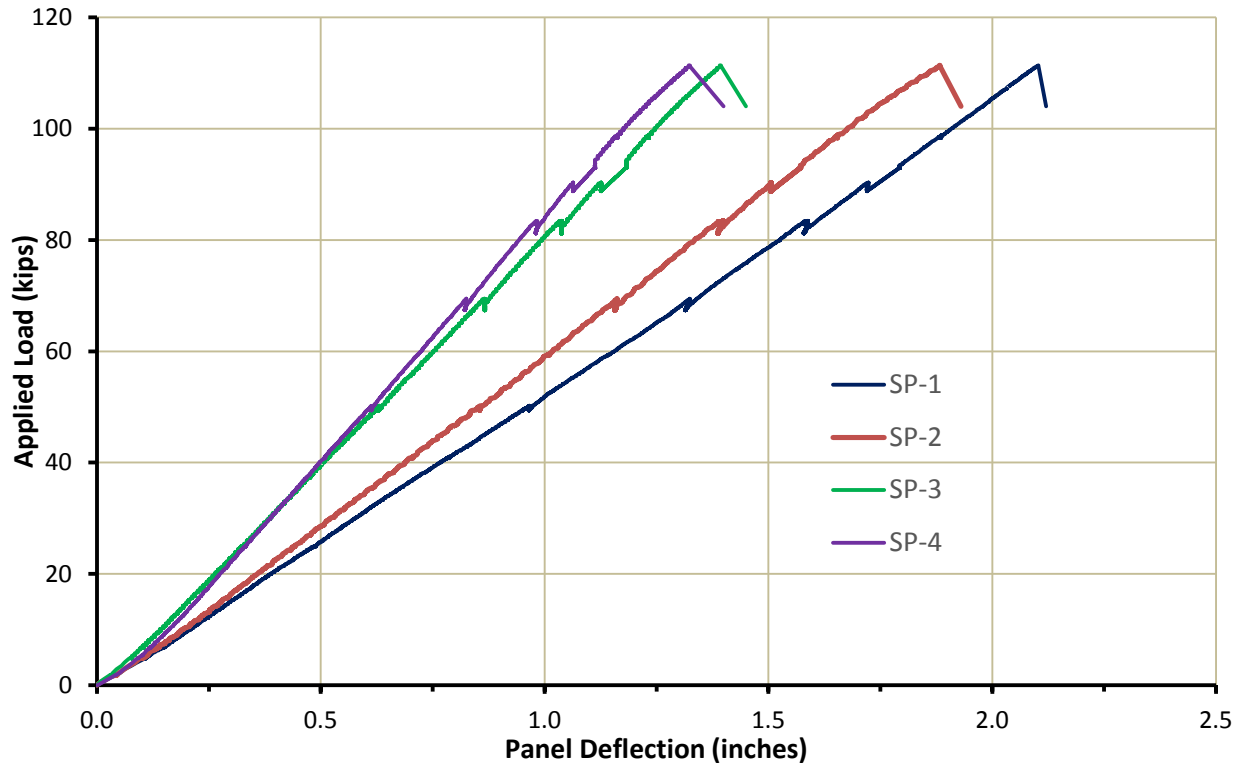
Figure 3.8: Load-Deflection Plot for Specimen FP-2 Flexural Test

Table 3.1: Summary of FRP Deck Specimen Flexural Tests

Specimen	Sequence No. 1		Sequence No. 2		Sequence No. 3	
	Load (kips)	Deflection (in)	Load (kips)	Deflection (in)	Load (kips)	Deflection (in)
FP1	21.3	0.418	37.2	0.717	108.9	2.077
FP2	21.3	0.411	37.2	0.712	111.4	2.103
FP3	21.3	0.404	37.2	0.695	104.2	1.931
Average	21.3	0.411	37.2	0.708	108.2	2.037
COV	-	1.7%	-	1.6%	3.4%	4.6%

The test summary information in **Table 3.1** also reveals a number of important characteristics with regard to the response and behavior of the prototype FRP deck panels. First, the results are very consistent between the three test specimens, with a maximum coefficient of variation (COV) of only 4.6%. This result indicates a consistency in the VARTM manufacturing process, which is very important with regard to the level of reliability in the industrial manufacturing of these panels for bridge decks. This low material response variability will also result in a small reduction in the capacity of the panel with regard to the resistance factor used in an LRFD design approach. Even more importantly, the average failure load exceeded the AASHTO Design Truck factored wheel load by nearly three times, 108.2 kips versus 37.2 kips, indicating a level of safety for these panels far beyond that required by code.

However, it is also important to note that the first series of panels manufactured for this research study suffered noticeable defects at the facesheet/web joint and near the panel edges. The likely cause of the voids at the facesheet/web joint was the presence of entrapped moisture, which vaporized during the curing process. Near the panel edges, a lack of complete resin saturation likely caused the defects. Corrective measures included extending the drying phase of the VARTM process and substituting a higher permeability distribution media. A thorough forensic evaluation revealed that subsequent panels exhibited no defects. All panels evaluated and reported on in this research study were fabricated with this revised VARTM process.

An important design issue for all bridge decks is the deflection under service load. The average service load deflection from **Table 3.1** is 0.411 in., which noticeably exceeds the customary AASHTO L/800 criteria (AASHTO LRFD, 2014). However, the FRP specimens for this testing program were designed based on strength, and traditionally, FRP decks have been limited by deflection control due to their very high strength to stiffness ratios. In other words, it is normal that deflection limits are the controlling limit state for an actual FRP bridge deck design (NAVFAC, 2005), but the intent of this testing program was to evaluate the design strength of the prototype FRP panels. Furthermore, the tested condition is a simply supported deck section, whereas in an actual bridge, the deck would be continuous over several longitudinal girders, which would reduce the deflection under live load. Also, recognizing that the L/800 limit is somewhat arbitrary and that the critical serviceability check involves debonding of the wearing surface (overlay), FHWA now recommends a deflection limit of L/500 for FRP bridge decks (FHWA, 2013).

The response and behavior of the test specimens is also revealed through the progression of images shown in **Figures 3.9** through **3.14**. **Figures 3.9** and **3.10** show specimen FP-1 under a load of 75 kips, or slightly more than two times the AASHTO Design Truck factored wheel load of 37.2 kips. Although the panel had undergone noticeable deformation, there were no signs of any distress or damage. In addition to inspecting the top and bottom facesheets, the research team also used flashlights and spotlights to inspect the multiple webs of the deck cross section. **Figures 3.11** and **3.12** contain images of specimen FP-1 immediately after failure. Although the panel has failed, it is still supporting a load of approximately 91 kips. Failure was initiated by local buckling of the compression flange (top facesheet) on each side of the applied concentrated load, which is clearly visible in **Figure 3.11**. A close-up of the buckled top facesheet is shown in

Figure 3.12, which reveals the separation between the top facesheet and the web elements. The ability to continue to support load is due to the post-buckling strength of the compression flange. However, additional application of load resulted in complete separation of the flange from the web, **Figures 3.13** and **3.14**, due to the presence of high transverse tensile stresses.

Fatigue is another important design issue for bridges due to the repetitive nature of traffic loading. As such, Phase I of this research included a fatigue flexural testing program. The protocol included two stress ranges and two limits on the number of cycles. The stress range limits were 20 percent and 45 percent of the ultimate load capacity, while the limits for the number of cycles were 1 million and 2 million. After fatigue testing, the panels were inspected for any signs of damage or distress, and then underwent static load testing to failure. None of the panels failed or even showed any visible signs of distress due to the fatigue loading, and they all surpassed the static load capacity of the control specimens. This result even held for the panels subjected to a 45 percent stress range for 2 million cycles, which represented a loading regime twice that required by the FRP guide specifications. The fatigue test results were also consistent with FRP bridge deck fatigue testing performed previously by a number of researchers (*e.g.*, Rocca and Nanni, 2005). In fact, as with the Phase I research, previous testing showed an increase in the panel stiffness and static load capacity due to reorganization of the polymer linkages during the cyclic loading phase (*e.g.*, Rocca and Nanni, 2005). As a result, fatigue testing was not deemed necessary for Phase II.

The measured strain values during the tests also offer valuable insight on the response and behavior of the deck panels. **Figure 3.15** is a plot of the measured strains in specimen FP-2 for gauges S-8, S-9, and S-2, which are located at midspan of the panel as shown in **Figure 3.3**. Gauges S-8 and S-9 are located on the tension flange (bottom facesheet) while gauge S-2 is located on the compression flange (top facesheet). Gauge S-2 is positioned immediately above gauge S-9. Consistent with the panel deformations, the measured strains also responded in a linear-elastic fashion throughout the full range of loading. Furthermore, in comparing gauges S-8 and S-9, there is only a 4% difference in the strain values just prior to failure (0.008190 in/in vs. 0.007896 in/in). Gauge S-8 is positioned at the panel centerline while gauge S-9 is positioned midway between the panel centerline and the edge. This small difference in strain readings between the two gauges again indicates a small amount of transverse curvature of the panel and nearly full engagement of the cross section to support the concentrated wheel load. Similar behavior also occurred at the panel quarter point, gauges S-11 and S-12 and gauges S-4 and S-5. Furthermore, the load-strain plots for gauges S-2 and S-9 – positioned in line vertically to each other – are nearly mirror images, which is consistent with the symmetrical panel cross section and offers additional confirmation of the validity of the strain gauge readings.
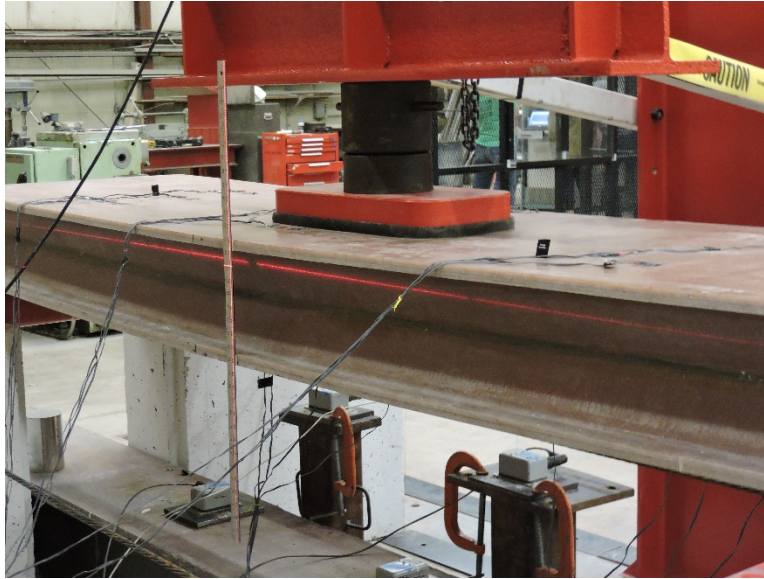
Figure 3.9: Specimen FP-1 During Flexural Test, 75 kip Load

Figure 3.10: Specimen FP-1 During Flexural Test, 75 kip Load

Figure 3.11: Local Buckling of Compression Flange, Specimen FP-1

Figure 3.12: Local Buckling of Compression Flange, Specimen FP-1
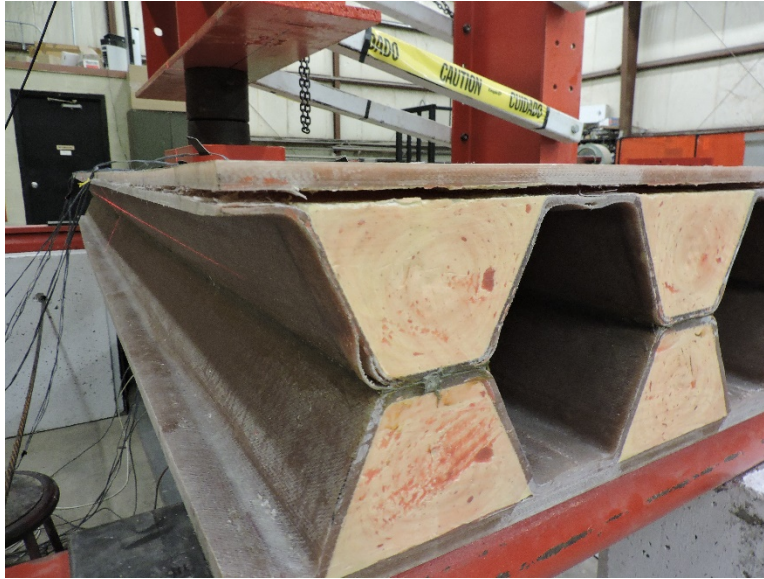
Figure 3.13: Separation of Compression Flange from Webs, Specimen FP-1
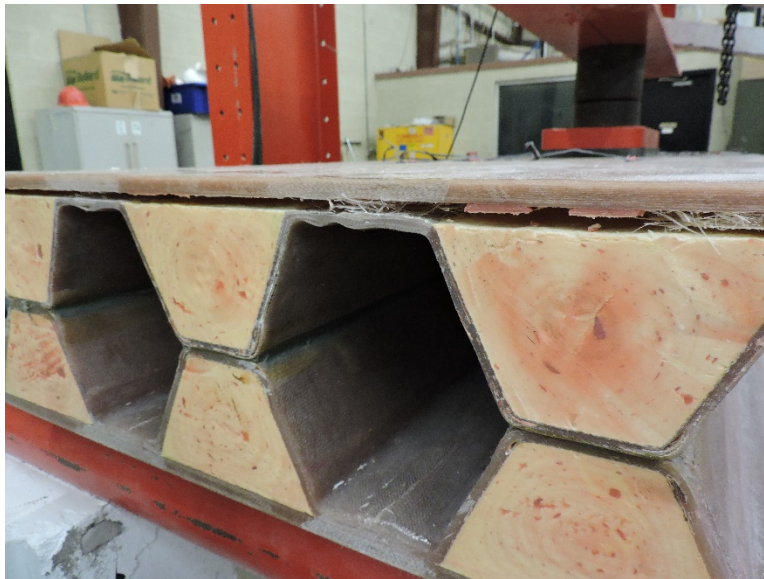
Figure 3.14: Separation of Compression Flange from Webs, Specimen FP-1
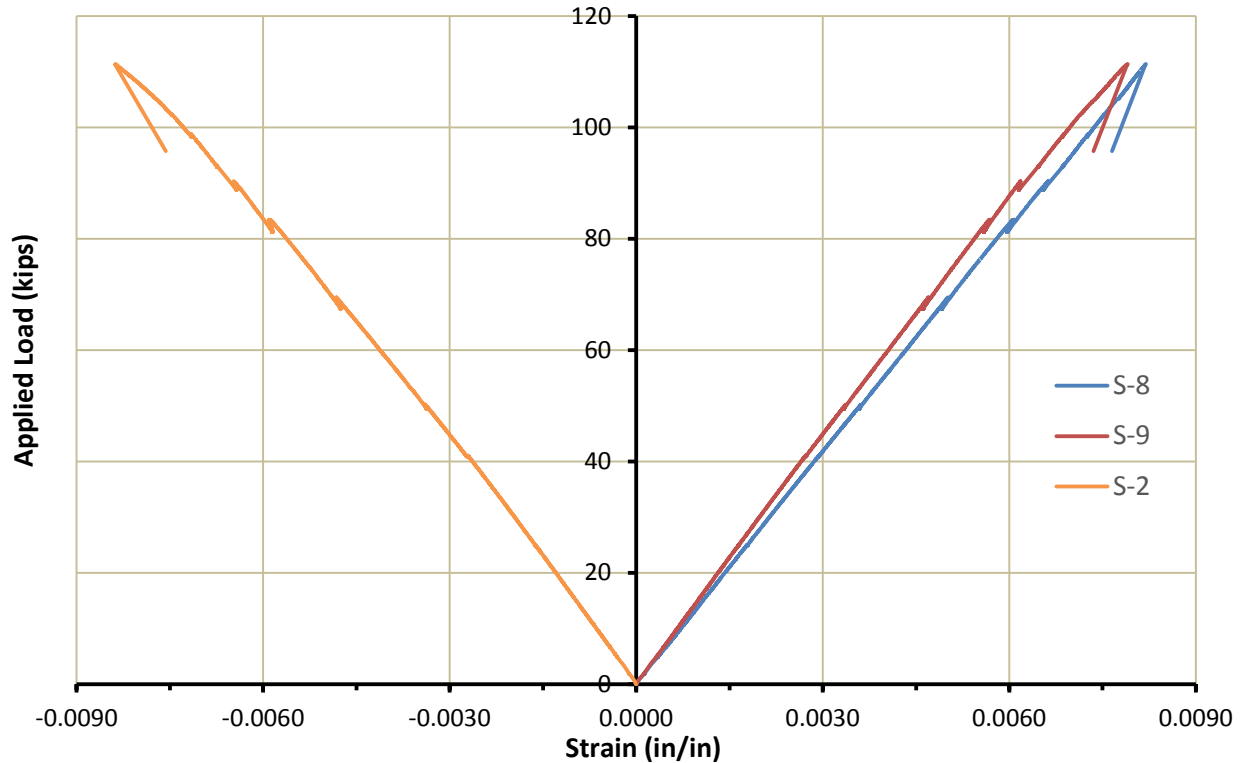
Figure 3.15: Load-Strain Plot for Specimen FP-2 Flexural Test

3.5. RESULTS OF SHEAR AND BEARING TESTS

The research team tested three (3) full scale, prototype FRP deck panels under a combination of shear and bearing following the test setup and loading protocol specified in Section 3.3. Overall, the panels were very consistent in terms of response and behavior. Failure was initiated by local buckling of the webs directly beneath the concentrated load point, which represents the point of application of the AASHTO Design Truck wheel load. The test specimens continued to support load after the webs buckled, and the panels returned to their original position after removal of the load, indicating no sustained damage. Based on this behavior, the loading protocol was revised during the test to include reloading of each specimen to determine if the panels retained their full strength or showed signs of degradation. A summary of the test results for the three (3) panels is provided in **Table 3.2**, and a typical cyclic load-deflection plot is shown in **Figure 3.16**.

FRP profiles are susceptible to local buckling under transverse loads due to the low in-plane moduli and the slenderness (width-to-thickness ratio) of the plate elements that comprise the cross sections. Both shearing stresses and bearing stresses may result in buckling of the webs of an FRP profile. In general, one of these modes will govern over the other depending on how the loads are applied. Under distributed loads, local buckling of the webs due to in-plane

shear will generally govern. However, under very high concentrated loads, such as those from a truck tire, local buckling of the webs due to in-plane bearing may govern. The test setup for the shear and bearing tests was developed to allow both modes to develop as a function of the applied AASHTO Design Truck loading. In other words, the loading setup would determine which mode governs for the prototype deck panel when subjected to the AASHTO loading requirements. Visual observations of the panels at failure revealed buckling of the webs directly beneath the concentrated load point, as shown in **Figures 3.17** and **3.18**. **Figure 3.17** shows the top facesheet depressing due to buckling of the underlying web, while **Figure 3.18** shows the buckled upper right sloping web immediately below the load point. All three (3) panels failed due to web buckling caused by excessive bearing stresses beneath the concentrated load.

Table 3.2: Summary of FRP Deck Specimen Shear and Bearing Tests

Specimen	Initial Loading Sequence to Failure		
	Applied Load (kips)	Maximum Shear (kips)	Bearing Load (kips)
SB1	125.7	104.0	125.7
SB2	134.9	111.6	134.9
SB3	117.1	96.9	117.1
Average	-	104.2	125.9
COV	-	7.1%	7.1%

The test summary information in **Table 3.2** reveals a number of important characteristics with regard to the response and behavior of the prototype FRP deck panels. First, as with the flexural test, the results for the shear and bearing test are very consistent between the three specimens, with a maximum coefficient of variation (COV) of only 7.1%. This result again indicates a consistency in the VARTM manufacturing process, which is very important with regard to the level of reliability in the industrial manufacturing of these panels for bridge decks. This low material response variability will also result in a small reduction in the capacity of the panel with regard to the resistance factor used in an LRFD design approach. Even more importantly, the average bearing failure load exceeded the AASHTO Design Truck factored wheel load by almost three and a half times, 125.9 kips versus 37.2 kips, indicating a level of safety for these panels far beyond that required by code.

Although the combined shear and bearing test indicated failure by excessive bearing stresses beneath the concentrated load, the test was useful in determining a lower bound for shear capacity. Since the panel did not fail in shear, the shear capacity is at least equal to the maximum shear in the panel at the point at which bearing failure occurred. As shown in **Table 3.2**, the average maximum shear value of 104.2 kips is 2.8 times the AASHTO Design Truck factored

wheel load of 37.2 kips. In other words, even with a complete AASHTO Design Truck factored axle load, consisting of two 37.2 kip wheel loads positioned on the panel at a spacing of 6 feet, the panel shear capacity exceeds the maximum shear force by a factor of 2.8, indicating a level of safety for these panels far beyond that required by code.
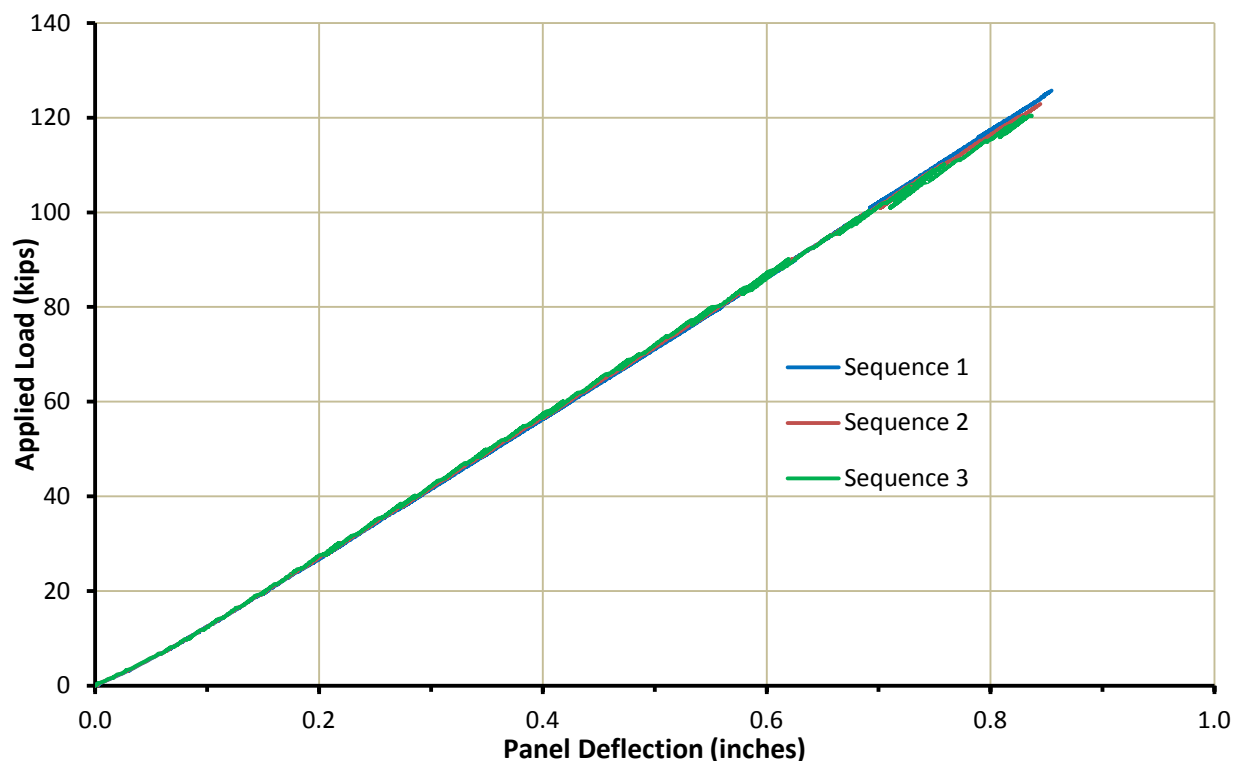
Figure 3.16: Cyclic Load-Deflection Plot for Specimen SB-1 Shear and Bearing Test

The load-deflection plot of **Figure 3.16** reveals a number of important characteristics with regard to the response and behavior of the prototype FRP deck panels. First, the revised loading protocol to include several cycles shows very little degradation with subsequent loading. This behavior is primarily a result of the failure mode of the panel, local buckling of the webs beneath the loading point. Buckling is generally an elastic response, so after the load is removed, the webs snap back into place without any permanent damage. This result is evident in the subsequent loading cycles which follow very nearly the same load-deflection path and fail very close to the initial loading value (125.7 kips vs. 122.9 kips vs. 120.3 kips). The only potential location for damage is at the joint between the webs and the top or bottom facesheet. The buckling failure may induce rotational stresses at the rigid connection between these elements, possibly tearing some of the fiberglass each time. Inspection of the web/facesheet interface did not show any signs of damage, but some microcracking could have occurred and would be exacerbated over time with multiple cycles. However, as mentioned previously, the peak load to

cause buckling of the webs (125.9 kips) is several times the AASHTO Design Truck factored wheel load of 37.2 kips, and thus the effect of any fatigue-type degradation due to multiple buckling failures is not a realistic scenario.

Figure 3.17: Top Facesheet Depressing Due to Buckled Web Below
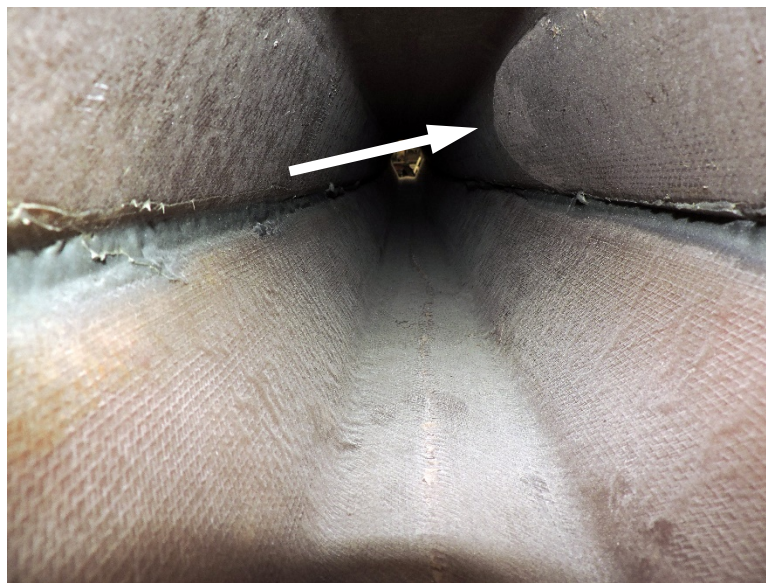
Figure 3.18: Buckling of Upper Right Sloping Web Located Below Load Point

3.6. SUMMARY

The research team tested six (6) full scale, prototype FRP deck panels in flexure, shear, and bearing. The results of the tests indicated that the panels significantly exceeded the code required design forces in all instances. In terms of flexure, the average failure load exceeded the AASHTO Design Truck factored wheel load by nearly three times, 108.2 kips versus 37.2 kips. In terms of bearing, the average failure load exceeded the AASHTO Design Truck factored wheel load by almost three and a half times, 125.9 kips versus 37.2 kips. In terms of shear, although the combined shear and bearing test indicated failure by excessive bearing, the coincident maximum shear force exceeded the maximum code specified shear force by a factor of 2.8, 104.2 kips versus 37.2 kips, based on the AASHTO Design Truck factored axle load consisting of two 37.2 kip wheel loads positioned on the panel at a spacing of 6 feet. Even more importantly, the panels behaved linearly-elastically throughout the full range of loading, indicating that excessive overstresses to the panels would not cause permanent damage or distress. The testing revealed that the prototype panel has a level of safety far beyond that required by the AASHTO design code. Also, since FRP decks are typically deflection controlled, an actual bridge deck based on the prototype panel would have an even higher margin of safety in terms of the strength limit states.

4. PANEL-TO-PANEL CONNECTION TESTING

The next task of the research study involved developing, manufacturing, testing, and evaluating alternative panel-to-panel connection methods for the prototype FRP deck panels. Unlike cast-in-place concrete, the FRP technology requires joining of the prefabricated panels on site to form the bridge deck. For a typical deck layout, the panels will span transversely to the direction of traffic, and the method of joining the panels must transfer sufficient load to prevent faulting when a vehicle passes from one panel to the next.

During the development stage, the research team investigated both mechanical and bonded methods of attaching the panels. All of the mechanical methods proved problematic. Preformed pockets to allow workers to site install and tension mechanical fasteners between the panels proved too costly. The pockets required extensive molding and localized reinforcement to insure panel integrity. Furthermore, preliminary testing indicated that a significant number of fasteners would be required to provide adequate load transfer, which rendered this option unworkable without a complete redesign of the prototype panel. Previous studies have also identified bolted panel-to-panel connections as considerably more expensive and difficult to achieve than adhesively-bonded connections (*e.g.*, Link, 2003; Zetterberg *et al.*, 2001).

In addition, previous research has shown that bolted panel-to-panel connections are more susceptible to fatigue loads than adhesively-bonded connections (*e.g.*, NAVFAC, 2005; Link, 2003; Zetterberg *et al.*, 2001). The primary reason stems from having to oversize the holes to allow fit-up during assembly. Under cyclic load tests, the bolts undergo movement and either fail prematurely in fatigue or cause the FRP to fail locally at the bolt hole location due to continual wear. As a result, the majority of FRP deck manufacturers have focused on adhesively-bonded panel-to-panel connections (Liu, 2007).

The research team studied several bonded methods of providing the panel-to-panel connection. These methods included forming keyways between adjacent panels as well as providing a simple butt-type connection. Preliminary tests of several keyway alternatives indicated very poor load transfer between adjacent panels. The keyway joints suffered several issues with regard to fit. Although capable of transferring load between adjacent panels, without a tight and secure fit, the panels suffered noticeable faulting prior to fully engaging.

Adhesively-bonded, butt-type connections have shown considerable promise in previous studies of FRP deck panels (Cassity *et al.*, 2002; Zetterberg *et al.*, 2001). These joints are more efficient in load transfer, have higher fatigue resistance, and are easier and less expensive to construct than mechanical connections. Martin Marietta Composites performed static, fatigue, and environmental durability tests on adhesively-bonded joints and showed that failure occurred exclusively in the composite material and not in the adhesive layer or interface (Liu, 2007).

Based on these previous studies as well as the preliminary work performed in this current work, the research team determined that a bonded butt-type connection offered the greatest potential for success. This type of joint required no modification to the prototype panel other than closing the cross-section to form a box, which would have been required anyway when the panels were developed for an actual bridge deck. The methacrylate structural adhesive selected

for the joints (Acralok SA10) has excellent fatigue and shock load resistance and is resistant to salt solutions, hydrocarbons, acids, and bases.

The following section discusses the specimen fabrication and characteristics, details of the test setup and loading protocol, and the response and behavior of the specimens under the required loading.

4.1. TEST PANEL FABRICATION

Working with Structural Composites and following the fabrication procedure discussed in Section 2, the research team manufactured three (3) full-scale, prototype FRP deck panel-to-panel connection pairs using a bonded butt-type joint. The panels were bonded using the same methacrylate adhesive used to fabricate the full prototype panel (see Section 2). Each individual panel of the bonded pair test specimen had the following characteristics:

- Depth: 9¼"
- Width: 3'– 0¼"
- Length: 5'– 0¼"

This panel width was again chosen to represent the minimum panel width that would be expected on an actual bridge layout and thus the smallest section size that would be required to support the axle load of an AASHTO Design Truck (AASHTO LRFD, 2014). The decreased panel length was chosen to reduce the ability of the panels to distribute load laterally to an absolute minimum and thus focus on the panel-to-panel joint performance. The dimensions of the cross section for one of the panels of the panel-to-panel test specimens are shown in **Figure 4.1**.
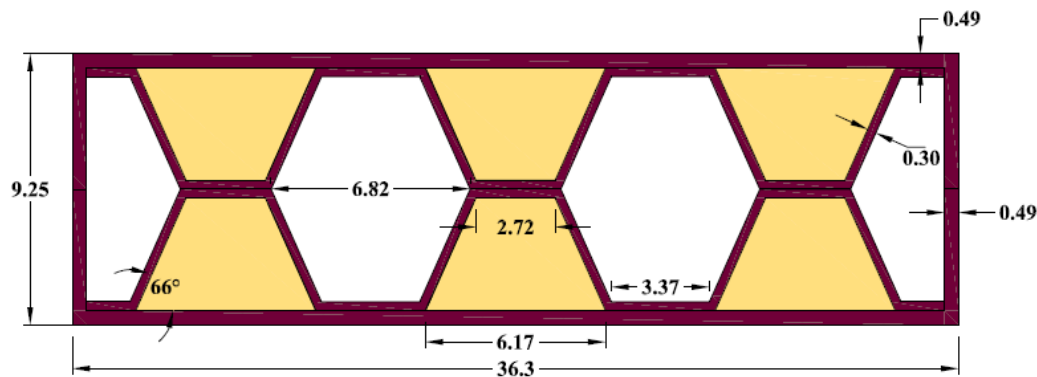
Figure 4.1: Full Scale Test Specimen Cross Section
(Note: all dimensions in inches)

4.2. TEST SETUP AND LOADING PROTOCOL

A schematic of the test setup is shown in **Figure 4.2**. The deck specimens are supported at each end by a concrete-filled steel tube to provide a roller support. A 1-in.-thick steel plate and

1/2-in.-thick rubber pad between the steel tube and deck specimens distributes the support reactions to prevent any stress concentrations. Concrete walls beneath the roller supports position the specimen at the required height within the load frame. Load is applied to the panels through a 300 kip Enerpac hydraulic ram and loading swivel. The loading swivel prevents stress concentrations as the panels deform under load. A 200 kip load cell is positioned between the hydraulic ram and loading swivel to record the applied force. The applied force is distributed to the deck through a 2-in.-thick steel plate measuring 10 in. along the direction of traffic and 20 in. perpendicular to the direction of traffic in accordance with the AASHTO specified truck tire contact area (AASHTO LRFD, 2014). A 1-in.-thick neoprene pad placed between the steel plate and the deck surface mimics the rubber tires of a truck and also prevents any stress concentrations at the loading point. The loading point was positioned at midspan along the centerline of one of the panels of the bonded pair.

Instrumentation for the test specimens is shown in **Figures 4.3** and **4.4**. **Figure 4.3** indicates the four spring potentiometers used to record the vertical deformation of the panels at midspan, with one positioned along each panel centerline and one positioned along each panel edge adjacent to the bonded joint. Strain gages were installed along the top and bottom facesheets of the panels as shown in **Figure 4.4**. A series of strain gauges were placed along each panel centerline and along each panel edge adjacent to the bonded joint, all measuring longitudinal strain. All of the instrumentation was recorded through a data acquisition system.

A photograph of an FRP deck panel-to-panel connection specimen within the test setup is shown in **Figure 4.5**. An arrow in the figure indicates the location of the bonded panel-to-panel joint.

Loading protocol for the panel-to-panel connection test involved a progression of loading sequences based on the wheel load for an AASHTO Design Truck (AASHTO LRFD, 2014). The Design Truck wheel load equals 21.3 kips based on one half of the 32 kip axle load increased 33% for the dynamic load allowance. With the Strength I live load factor of 1.75, the full factored wheel load equals 37.2 kips. The loading sequences consisted of the following:

- Sequence No. 1: Load from zero to 21.3 kips (AASHTO Design Truck wheel load) then return to zero

- Sequence No. 2: Load from zero to 37.2 kips (AASHTO factored Design Truck wheel load) then return to zero

- Sequence No. 3: Load from zero to failure

The protocol consisted of three repetitions of Sequence No. 1, followed by three repetitions of Sequence No. 2, and then finished with testing the panel to failure, Sequence No. 3. At the end of each sequence, the panels were inspected for any signs of damage.

(a) Elevation View
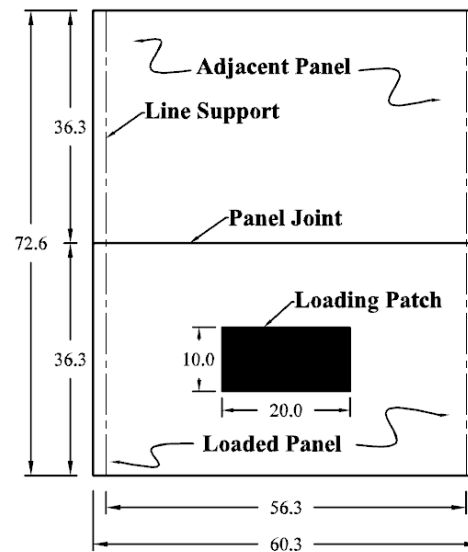
(b) Plan View

Figure 4.2: Schematic of Panel-to-Panel Connection Test Setup
(Note: all dimensions in inches)
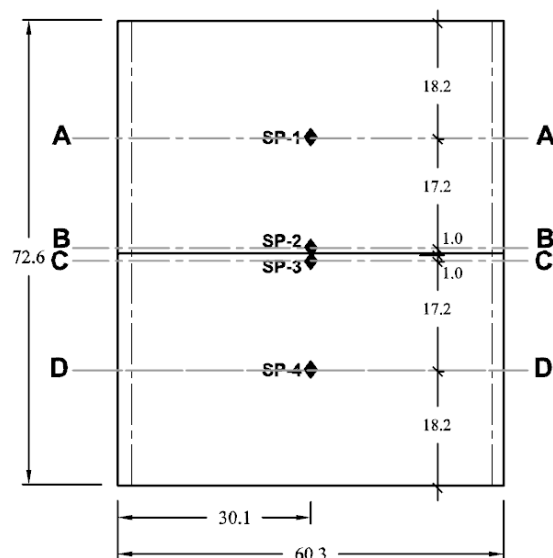
Figure 4.3: Spring Potentiometer Instrumentation for Panel-to-Panel Connection Test Specimens (Note: all dimensions in inches)

4.3. RESULTS OF PANEL-TO-PANEL CONNECTION TESTS

The research team tested three (3) full scale, prototype FRP deck panel-to-panel connection pairs following the test setup and loading protocol specified in Section 4.2. Overall, the specimens were very consistent in terms of response and behavior. Failure was initiated by local buckling of the webs directly beneath the concentrated load point, which represents the point of application of the AASHTO Design Truck wheel load. However, unlike the flexure, shear, and bearing load tests (Section 3), the panels revealed non-linear load-deflection behavior at higher loads, indicating some inelastic response of the panel-to-panel joint and possibly a slight loss of load sharing between the two panels. A typical load-deflection plot for one of the FRP deck panel-to-panel connection specimens is shown in **Figure 4.6**.

During the three repetitions of loading Sequence No. 1 (zero to 21.3 kips) and the three repetitions of loading Sequence No. 2 (zero to 37.2 kips), the deflections on each side of the panel joint (SP-2 and SP-3) were essentially identical, and the load-deflection response was linear-elastic. However, during the loading for Sequence No. 3 (zero to failure), the panels began to show non-linear behavior at a load of approximately 80 kips, as shown in **Figure 4.6** for specimen PTP-3. This behavior was contrary to that experienced by the flexure, shear, and bearing test specimens. As a result, it is likely that the panel-to-panel joint began to experience some inelastic response, causing a decrease in the amount of load transferred from the loaded panel to the adjacent panel. Inspection of the joint during loading Sequence No. 3 revealed no signs of damage or distress. It is possible that the methacrylate adhesive began to undergo inelastic shearing deformations, which reduced the rigidity of the joint and caused a decrease in load transfer to the adjacent panel.
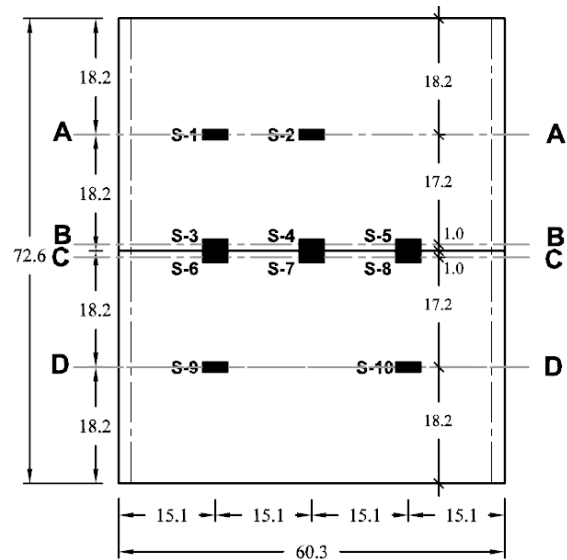
(a) Top Facesheet Strain Gauge Layout
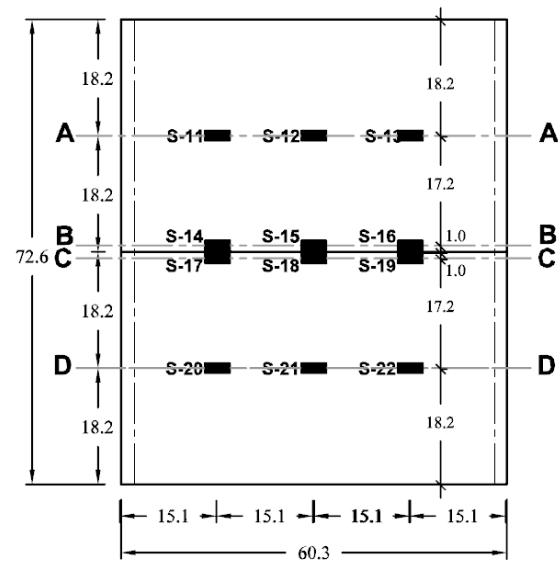
(b) Bottom Facesheet Strain Gauge Layout

Figure 4.4: Strain Gauge Instrumentation for Panel-to-Panel Connection Test Specimens (Note: all dimensions in inches)
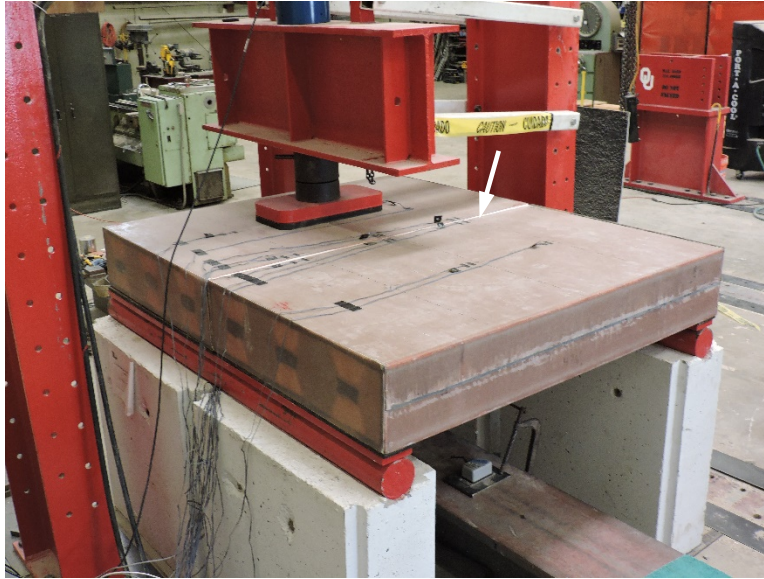
Figure 4.5: Panel-to-Panel Connection Test Setup for FRP Deck Specimens
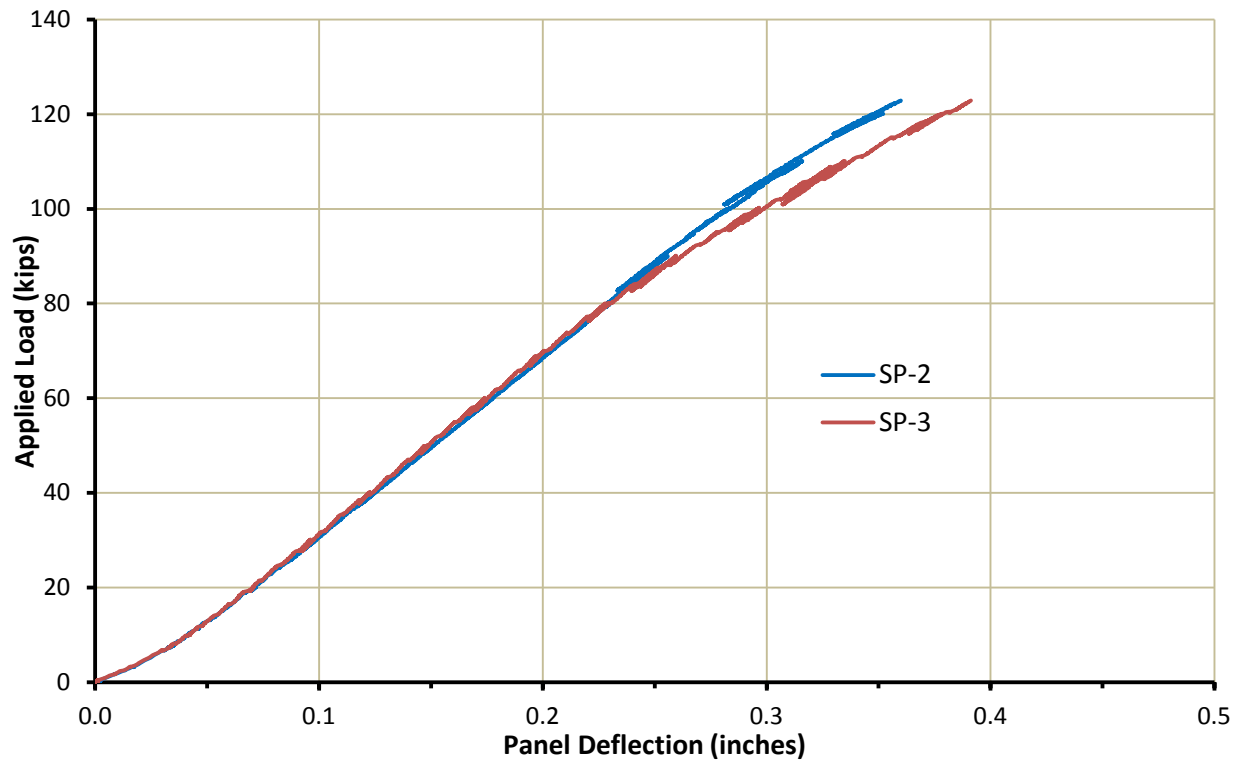
Figure 4.6: Load-Deflection Plot for Specimen PTP-3 Panel-to-Panel Connection Test

However, it is important to note that the measurements indicated 100% load transfer from the loaded panel to the adjacent panel up to a load of approximately 80 kips, or a little over twice the AASHTO Design Truck factored wheel load of 37.2 kips. In other words, the bonded joint provided 100% load transfer well beyond that required by code. Furthermore, the panel-to-panel joint never failed in terms of strength, providing significant load transfer to the adjacent panel during the full range of loading. **Figures 4.7** and **4.8** are photographs of specimen PTP-1 immediately after the bearing failure. The panel is supporting a load of approximately 93 kips after the webs buckled beneath the load point at a peak of 122.9 kips (note the depressed top facesheet around the loading point). There is no discernable faulting between the panels or failure of the bonded joint.

4.4. SUMMARY

Testing of a bonded butt-type panel-to-panel connection for the prototype FRP deck panels indicated 100% load transfer up to a load of approximately 80 kips, or a little over twice the AASHTO Design Truck factored wheel load of 37.2 kips. After 80 kips, the methacrylate adhesive began to undergo inelastic shearing deformations, which reduced the rigidity of the joint and caused a decrease in load transfer to the adjacent panel. However, the panel-to-panel joint never failed in terms of strength, providing significant load transfer to the adjacent panel up to the point at which the loaded panel failed due to local buckling of the webs beneath the load point.
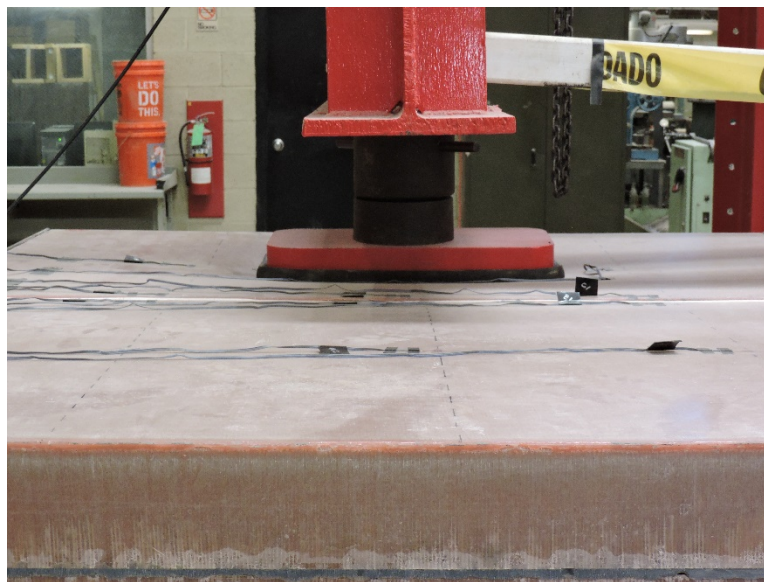
Figure 4.7: Specimen PTP-1 During Panel-to-Panel Connection Test, 93 kip Load
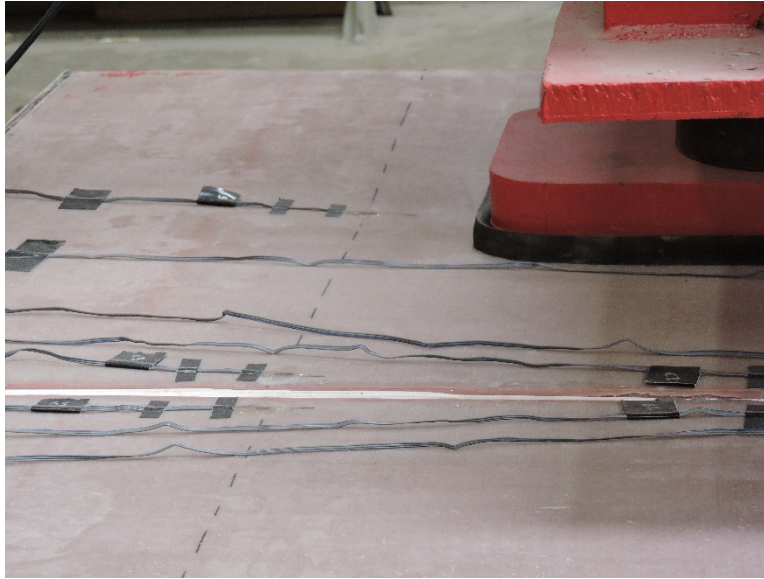
Figure 4.8: Specimen PTP-1 During Panel-to-Panel Connection Test, 93 kip Load

5. GUARDRAIL-TO-PANEL CONNECTION TESTING

FHWA requires that bridge railings undergo full-scale crash testing following guidelines established in NCHRP Report 350 or the AASHTO Manual for Assessing Safety Hardware (MASH). FHWA maintains a database of accepted railings and also provides analytical procedures to evaluate similar railings without having to perform full-scale crash testing. Provided the approved guardrails are attached to the FRP deck panels in the same fashion, full scale crash testing is not required (FHWA, 2013; NCHRP, 2002; Alampalli *et al.*, 2000). Instead, a static load test based on the requirements specified in the AASHTO *LRFD Bridge Design Specifications* (AASHTO LRFD, 2014) is acceptable in determining performance of the deck. As a result, this task involved manufacturing full scale, prototype FRP deck panels followed by testing and evaluating the panels for the design loads specified within the AASHTO code. The following section discusses the specimen fabrication and characteristics, details of the test setup and loading protocol, and the response and behavior of the specimens under the required loading.

5.1. TEST PANEL FABRICATION

Again working with Structural Composites and following the fabrication procedure discussed in Section 2, the research team manufactured three (3) full-scale, prototype FRP deck sections for guardrail testing. The deck panels had the following characteristics:

- Depth: 9¼"
- Width: 2'–5½"
- Length: 10'–1"

This panel width was again chosen to represent the minimum panel width that would be expected on an actual bridge layout and thus the smallest section size that would be required to support an individual guardrail post. The panel width determines the effective section able to support the loads imposed during the test and during an actual vehicular collision. The complete dimensions of the cross section for the full scale test specimens are shown in **Figure 5.1**.
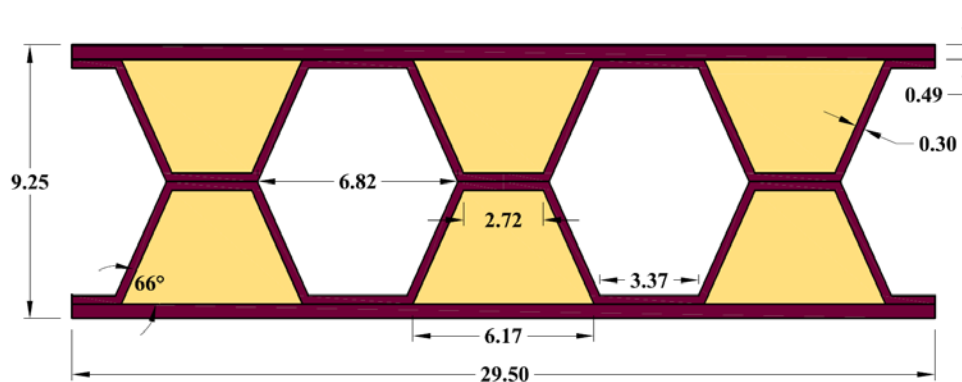
Figure 5.1: Full Scale Test Specimen Cross Section
(Note: all dimensions in inches)

5.2. TEST SETUP AND LOADING PROTOCOL

A schematic of the test setup is shown in **Figure 5.2**. The deck specimens are supported to mimic the typical deck overhang condition of a bridge. Concrete-filled steel tubes provide a line of support to represent the edge girder and the first interior girder. To prevent any stress concentrations, 1-in.-thick steel plates and 1/2-in.-thick rubber pads were positioned between the steel tubes and deck specimen. The guardrail post – termed an "on top mount" – consists of an HSS6x6x1/2 steel section welded to a 3/4-in.-thick steel plate and through-bolted to the panel with four 3/4-in.-diameter bolts. Support at the first interior girder includes a hold down point to resist the uplift force generated from the overturning moment during loading. The required horizontal load is applied to the guardrail post through a 100 kip Enerpac hydraulic pull cylinder positioned at a height of 24 in. above the top of the deck. This height coincides with the recommended loading position for an AASHTO Test Level 3 (TL-3) guardrail safety performance (AASHTO LRFD, 2014). A 100 kip load cell is positioned between the cylinder and the attachment to the guardrail post to record the applied force.

The only instrumentation for the test consists of the load cell positioned in line with the hydraulic cylinder. As it was believed that the failure would be highly localized, strain gauges would not provide any beneficial information. Furthermore, since the loading is to mimic a vehicular crash, displacements were not deemed critical to the performance of the panel during the test, particularly since there are no AASHTO requirements on deformation during the loading sequence. The load cell data was recorded through a data acquisition system.

Loading protocol for the guardrail connection test involved loading the vertical post from zero to failure in increments of 5 kips. After each increment of load, the research team inspected the panel for any signs of damage or distress.

A photograph of an FRP deck specimen within the test setup is shown in **Figure 5.3**.

5.3. RESULTS OF GUARDRAIL CONNECTION TESTS

The research team tested the guardrail-to-panel connection for three (3) full scale, prototype FRP deck panels following the test setup and loading protocol specified in Section 6.2. Overall, the panels were very consistent in terms of response and behavior. Failure was initiated by local crushing of the FRP at the bolt holes within the top facesheet – a bearing-type failure where the strength of the material was exceeded under localized compression. This failure mode is primarily one of localized excessive deformation. The load plateaued but did not suffer any decrease in value. The top of the guardrail post (loading point) simply continued to deflect horizontally once the peak load was reached. Eventually, localized tearing of the FRP top facesheet from the webs would have occurred. A summary of the test results for the three (3) panels is provided in **Table 5.1**.

Figures 5.4 through **5.6** show the results of one of the panels subjected to the guardrail test. **Figure 5.4** is a photograph of specimen GP1 at the peak load of 27.48 kips, which displays bowing of the panel, slight uplift of the base plate, but no signs of any global failure of the panel. **Figure 5.5** shows the localized bearing failure at the location of one of the through-bolt holes in

the panel top facesheet for specimen GP1. Note the indentations of the bolt threads in the FRP top facesheet, which would be eliminated through the use of bolts with threads located outside of the bearing area. **Figure 5.5** also reveals the localized bearing failure along the top edge of the facesheet (highlighted with arrows in the figure). **Figure 5.6** indicates the potential start of a tearing failure between the top facesheet and webs at the bolt hole locations (highlighted with arrows in the figure).
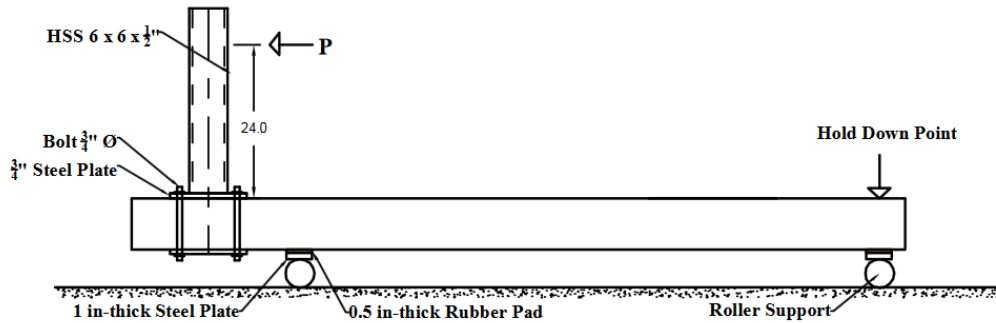
(a) Elevation View
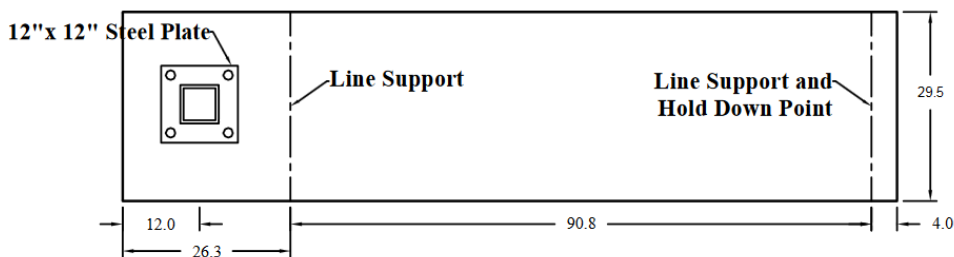
(b) Plan View

Figure 5.2: Schematic of Guardrail-to-Panel Connection Test Setup
(Note: all dimensions in inches)

As shown in **Table 5.1**, the average peak load measured 30.37 kips, which exceeded the 27 kip factored transverse design load for the AASHTO TL-2 guardrail safety performance (AASHTO LRFD, 2014). AASHTO level TL-2 covers work zones and most local and collector roads as well as where a small number of heavy vehicles is expected and posted speeds are reduced. To attain AASHTO levels TL-3 and TL-4 would require locally reinforcing the panels at the connection points of the guardrail posts. Based on the panel flexural testing (Section 3), the prototype deck panel has sufficient moment capacity to resist the required guardrail post flexural moment for AASHTO level TL-4, a 255 ft-kip capacity versus a 144 ft-kip factored moment (54 kips at a height of 32 in.).

However, the basis for this comparison assumes a 4 foot post spacing for the guardrail system and 100% of the horizontal load supported by a single post, which is very conservative. The horizontal members of a guardrail system will distribute the impact load among several guardrail posts, reducing the value for any individual vertical support. Nonetheless, locally reinforcing the panels at the guardrail post connection points will easily increase the panel capacity at a relatively low cost. One potential method to reinforce the panels and prevent a bearing-type failure would include placing steel pipe sleeves at the through-bolt hole locations and locally increasing the thickness of the top and bottom facesheets.

Figure 5.3: Guardrail-to-Panel Connection Test Setup for FRP Deck Specimens

Table 5.1: Summary of Guardrail-to-Panel Connection Tests

Specimen	Load Height (in)	Peak Load (kips)
GP1	24.0	27.48
GP2	24.0	31.22
GP3	24.0	32.41
Average	-	30.37
COV	-	8.5%
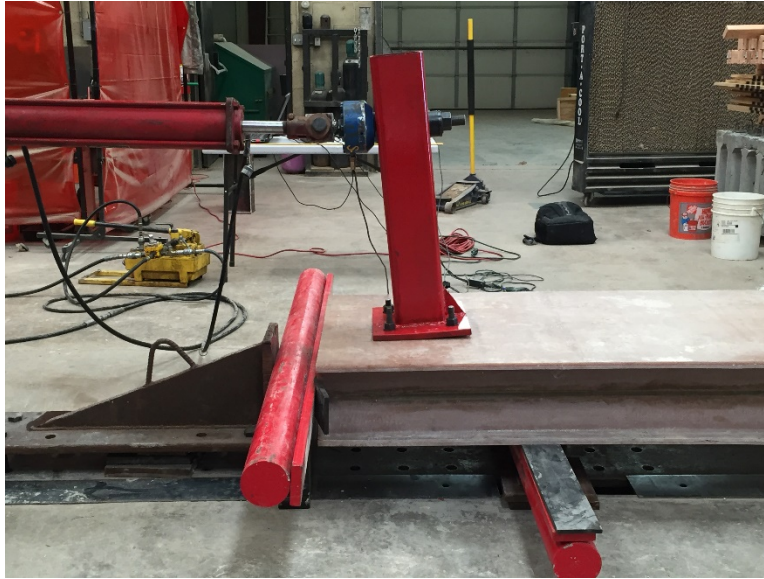
Figure 5.4: Specimen GP-1 During Guardrail-to-Panel Connection Test
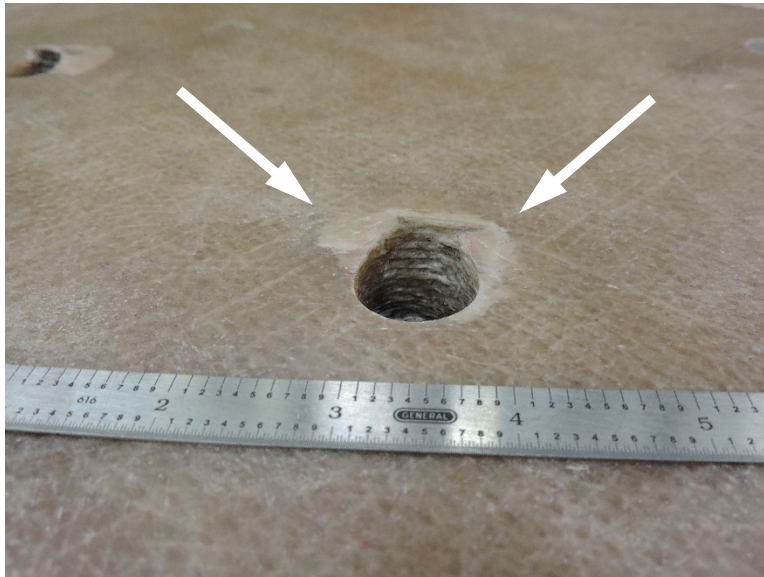
Figure 5.5: Bearing Failure at Bolt Hole Location of Specimen GP-1 Top Facesheet
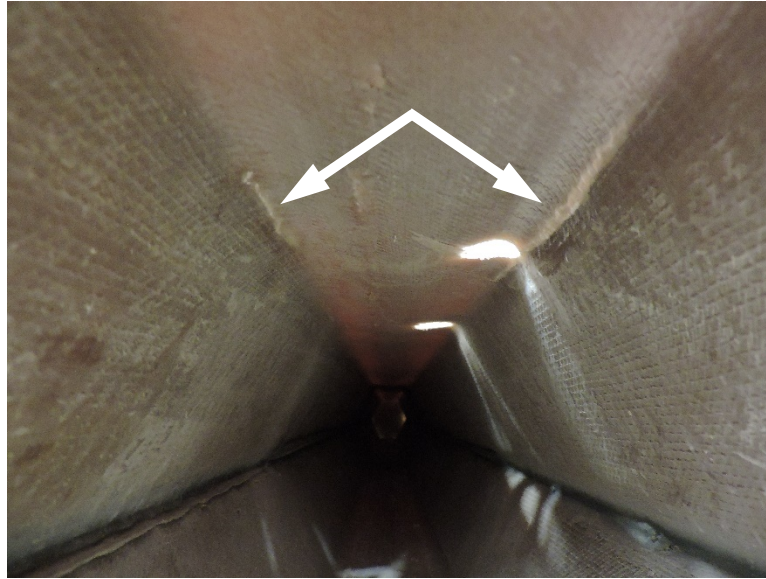
**Figure 5.6: Signs of Potential Tearing Failure Between Facesheet
and Webs, Speciment GP-1**

5.4. SUMMARY

Testing of the guardrail-to-panel connection for the prototype FRP deck panels indicated that without any modifications, the panels satisfy the AASHTO TL-2 guardrail requirements. Based on the panel flexural testing (Section 3), the prototype deck panel also has sufficient inherent moment capacity to resist the required guardrail post flexural moment for AASHTO level TL-4 (54 kips at a height of 32 in.). As a result, to attain an AASHTO TL-3 or TL-4 level, the panels would only require localized reinforcement at the guardrail post connection points, which is very common in FRP bridge deck construction. One potential method to increase capacity and prevent a bearing-type failure would include placing steel pipe sleeves at the through-bolt hole locations and locally increasing the thickness of the top and bottom facesheets. Other methods to locally reinforce the connection points are also possible. Most importantly, the overall panel design would not need to change to attain a TL-3 or TL-4 level.

The issue of requiring a full scale crash test of the railing/FRP deck combination is unsettled. Some studies (FHWA, 2013; NCHRP, 2002; Alampalli *et al.*, 2000) have supported the approach taken in this current research effort while others have advocated for a full scale crash test program (*e.g.*, El-Aasar, 2015). As a compromise, a bogie test may be an acceptable alternative (El-Aasar, 2015; NCHRP, 2002).

6. COMPARISON OF FULL SCALE TEST RESULTS TO DESIGN EQUATIONS

The next task of the research study involved comparing the results of the full scale panel tests to existing design equation for FRP materials. The VARTM process, discussed in detail in Section 2, is common in the automobile, marine, and industrial sectors. However, the design methodology for VARTM-constructed parts has not been quantified for transportation applications within civil engineering. The following section evaluates the applicability of existing FRP design equations when used for the design of the VARTM-manufactured, prototype FRP bridge deck.

6.1. GENERAL

For FRP cross sections, the critical ultimate limit states involve both direct material failures and local buckling failures. The local buckling limit states are the result of the low in-plane moduli and slenderness (width-to-thickness ratio) of the plate elements that comprise the cross section. For the prototype section, lateral-torsional buckling is not an applicable limit state due to the much larger width of the panels compared to their depth. As a result, the following limit states are applicable to the FRP bridge deck:

- Compressive, tensile, and shear strength material failures
- Local buckling of the flange or webs due to in-plane compression
- Local buckling of the webs due to in-plane shear
- Local crushing or buckling of the webs due to concentrated loads

The dimensions of the prototype FRP deck cross section for use in evaluating the design equations are shown in **Figure 6.1**, and the material properties based on the fabrication process discussed in Section 2 are shown in **Table 6.1**. Refer to **Figures 2.2** through **2.6** for a schematic representation of the prototype FRP deck fabrication process and layout of the different fabric types listed in **Table 6.1**.
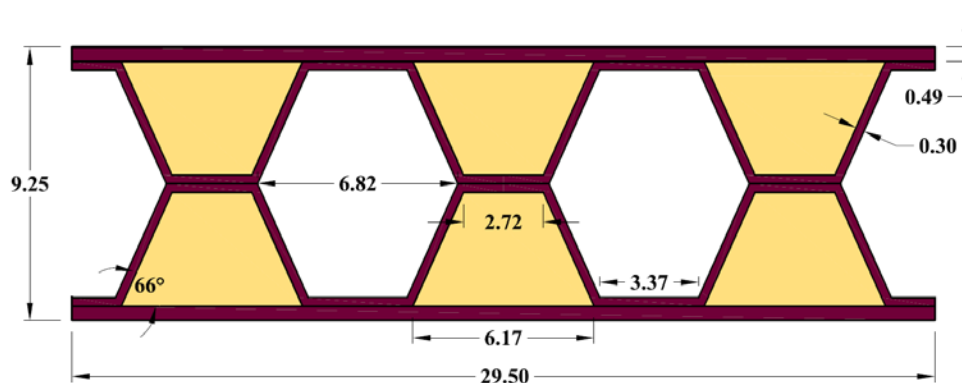
Figure 6.1: Prototype FRP Deck Cross Section
(Note: all dimensions in inches)

Table 6.1: Prototype FRP Deck Material Properties

Property	Fabric 1 E-LM 1810 (90°)	Fabric 2 E-LM 1810 (0°)	Fabric 3 E-BXM 1715 (+45°/−45°)
Longitudinal Modulus, E_L (0°)	1,640 ksi	3,870 ksi	2,830 ksi
Transverse Modulus, E_T (90°)	3,870 ksi	1,640 ksi	2,830 ksi
Shear Modulus, G_{LT} (+45°/−45°)	720 ksi	720 ksi	590 ksi
Longitudinal Tensile Strength, $\sigma_{L,t}$ (0°)	26.8 ksi	63.5 ksi	46.5 ksi
Longitudinal Compressive Strength, $\sigma_{L,c}$ (0°)	31.0 ksi	73.3 ksi	64.6 ksi
Transverse Tensile Strength, $\sigma_{T,t}$ (90°)	63.5 ksi	26.8 ksi	46.5 ksi
Transverse Compressive Strength, $\sigma_{T,c}$ (90°)	73.3 ksi	31.0 ksi	64.6 ksi
In-Plane Shear Strength, τ_{LT} (+45°/−45°)	16.3 ksi	16.3 ksi	13.4 ksi

The prototype FRP deck cross section shown in **Figure 6.1** is fabricated from a number of individual stacked plies of fabric subsequently infused with a resin. The process for the prototype deck is discussed in detail in Section 2. As a result, the longitudinal and transverse properties of the full cross section are a function of the type, number, orientation, and properties of the individual resin-infused laminates. These transverse and longitudinal properties can be determined using the rule of mixtures, such as that shown in **Equation 6.1** for determining the longitudinal modulus of elasticity, E_L.

$$\frac{1}{E_L} = \sum_{i=1}^{n} \frac{v_i}{(E_L)_i} \tag{6.1}$$

where v_i and $(E_L)_i$ are the volume fraction and longitudinal modulus of elasticity for the *ith* laminate, respectively.

The top and bottom facesheets contain six laminates of Fabric 1 and six laminates of Fabric 2, which are identical fiberglass fabrics except for the orientation. Fabric 1 has the strong

axis oriented in the transverse direction of the panel while Fabric 2 has the strong axis oriented in the longitudinal direction. As a result, the top and bottom facesheets are isotropic with regard to in-plane stresses. Applying the rule of mixtures provides the following moduli and material strengths for the top and bottom facesheets:

$$\frac{1}{E_L} = \left(\frac{0.5}{1,640\ ksi}\right) + \left(\frac{0.5}{3,870\ ksi}\right)$$

$$E_L = 2,304\ ksi$$

$$E_T = E_L = 2,304\ ksi$$

$$\frac{1}{\sigma_{L,t}} = \left(\frac{0.5}{26.8\ ksi}\right) + \left(\frac{0.5}{63.5\ ksi}\right)$$

$$\sigma_{L,t} = 37.7\ ksi$$

$$\sigma_{T,t} = \sigma_{L,t} = 37.7\ ksi$$

$$\frac{1}{\sigma_{L,c}} = \left(\frac{0.5}{31.0\ ksi}\right) + \left(\frac{0.5}{73.3\ ksi}\right)$$

$$\sigma_{L,c} = 43.6\ ksi$$

$$\sigma_{T,c} = \sigma_{L,c} = 43.6\ ksi$$

where E_L and E_T are the longitudinal and transverse moduli of elasticity, respectively, $\sigma_{L,t}$ and $\sigma_{T,t}$ are the longitudinal and transverse ultimate tensile strengths, respectively, and $\sigma_{L,c}$ and $\sigma_{T,c}$ are the longitudinal and transverse ultimate compressive strengths.

The webs consist of four laminates of Fabric 3, which is a symmetrical fabric and, as a result, the webs are also isotropic for in-plane stresses, and the moduli and material strengths are provided in **Table 6.1** directly.

The peak force effects to compare with the existing FRP design equations are summarized in **Table 6.2**. It is important to note that the test specimens failed in flexure and bearing, but that it was not possible to reach a shear failure ultimate state as the bearing failure occurred first, which is typical for FRP cross sections subjected to large concentrated forces.

Table 6.2: Peak Force Effects from Full Scale Panel Tests

Design Force	Peak Test Value	Notes
Flexure	2,785 in-k	local buckling of top facesheet
Shear	111.6 k	panel failed in bearing prior to shear failure
Bearing	134.9 k	local buckling of webs beneath load point

6.2. COMPRESSIVE, TENSILE, AND SHEAR STRENGTH MATERIAL FAILURES

For FRP members where the slenderness ratios of the flange and web are small and local buckling does not occur, the member may fail due to tensile rupture, compressive crushing, or in-plane shear failure. For a material tensile failure due to flexure, the critical tensile stress is taken as the longitudinal ultimate tensile strength. For a material compressive failure due to flexure, the critical compressive stress is taken as the longitudinal ultimate compressive strength. Finally, for a material in-plane shear failure due to transverse loads, the critical shear stress is taken as the ultimate in-plane shear strength. Unlike buckling stresses, any interaction between in-plane normal and shear stresses is not generally considered in the design of FRP members (Bank, 2006). As a result, the following design values are obtained:

$$\sigma_{cr}^{ten} = \sigma_{L,t} = 37.7 \; ksi$$

$$\sigma_{cr}^{comp} = \sigma_{L,c} = 43.6 \; ksi$$

$$\tau_{cr}^{shear} = \tau_{LT} = 13.4 \; ksi$$

The critical moments and shears can then be calculated using traditional one-dimensional beam theory, repeated as Equations 6.2 through 6.4:

$$M_{cr}^{ten} = \sigma_{cr}^{ten} \frac{I_x}{y} \tag{6.2}$$

$$M_{cr}^{comp} = \sigma_{cr}^{comp} \frac{I_x}{y} \tag{6.3}$$

$$V_{cr} = \tau_{cr}^{shear} \frac{I_x t}{Q} \cong \tau_{cr}^{shear} A_{web} = \tau_{cr}^{shear} t_w d_w \tag{6.4}$$

Since the cross section is symmetric, tension will govern for the flexural check, and the critical moment and shear are the following:

$$M_{cr}^{ten} = (37.7) \left(\frac{753.0}{(9.25/2)} \right) = 6,138 \; in\text{-}k$$

$$V_{cr} = (13.4)[(6 \; webs)(0.3)(2(4.562))] = 219.8 \; kips$$

Both values comfortably exceed the peak force effects from **Table 6.2**, which is consistent with the fact that no material tensile rupture of the bottom facesheet or shear failure of the webs was observed during the tests.

6.3. LOCAL BUCKLING OF THE FLANGE OR WEBS DUE TO IN-PLANE COMPRESSION

FRP profiles are susceptible to local buckling under transverse loads due to the low in-plane moduli and the slenderness (width-to-thickness ratio) of the plate elements that comprise the cross sections. Both the flange and the web may buckle due to in-plane compressive stresses generated from the applied bending moment. For the flange, these normal

stresses are uniform while for the web, these normal stresses vary linearly from zero at the neutral axis to a peak value at the intersection with the flange. In addition to the applied stress distribution, the critical buckling stress is also a function of the boundary conditions along the longitudinal edges of the flange or web. For instance, in an I-shaped cross section, the flange is free along one edge while the other edge is elastically restrained where the flange and web meet. However, for a box section, the flange is elastically restrained along both longitudinal edges. Webs for I-shaped and box sections are restrained along both longitudinal edges.

The degree of elastic restraint along the supported edge of a flange is a function of the characteristics of the web providing that support. Similarly, the degree of elastic restraint along the edge of a web is a function of the characteristics of the flange providing that support. The approach to determining the critical buckling stress of the flange or web is to assume that they are simply supported along their restrained edges. The resulting buckling stresses are then compared to determine whether the flange or web buckles first. The degree of restraint provided by the non-buckling element is than determined, and this modified restraint is then used to calculate a revised buckling stress for the critical element. As such, the buckling stresses for the flange and the web of a box section assuming simply supported edges are calculated using Equations 6.5 and 6.6, respectively. The values are a function of the flexural rigidities, D.

$$(\sigma_{ss}^{ss})_f = \left(\frac{2\pi^2}{t_f b_f^2}\right)\left(\sqrt{D_L D_T} + D_{LT} + 2D_S\right) \tag{6.5}$$

$$(\sigma_{ss}^{ss})_w = \left(\frac{\pi^2}{t_w d_w^2}\right)\left(13.9\sqrt{D_L D_T} + 11.1D_{LT} + 22.2D_S\right) \tag{6.6}$$

where D_L, D_T, D_{LT}, and D_s are the longitudinal, transverse, coupling, and shear flexural rigidities (plate flexural rigidities), respectively, t_f and b_f are the flange thickness and effective width, respectively, and t_w and d_w are the web thickness and effective depth, respectively.

For the flange of the prototype FRP deck section,

$$D_L = D_T = \frac{E_L t_f^3}{12(1 - v_L v_T)} = \frac{(2,304,000)(0.49)^3}{12(1 - (0.33)(0.33))} = 25,349 \; lb\text{-}in$$

$$D_{LT} = v_T D_L = (0.33)(25,349) = 8,365 \; lb\text{-}in$$

$$D_S = \frac{G_{LT} t_f^3}{12} = \frac{(720,000)(0.49)^3}{12} = 7,059 \; lb\text{-}in$$

$$(\sigma_{ss}^{ss})_f = \left(\frac{2\pi^2}{(0.49)(6.27)^2}\right)\left(\sqrt{(25,349)^2} + 8,365 + 2(7,059)\right) = 46,030 \; psi$$

For the web of the prototype FRP deck section,

$$D_L = D_T = \frac{E_L t_w^3}{12(1 - v_L v_T)} = \frac{(2,830,000)(0.3)^3}{12(1 - (0.33)(0.33))} = 7,145 \; lb\text{-}in$$

$$D_{LT} = v_T D_L = (0.33)(7,145) = 2,358 \ lb\text{-}in$$

$$D_S = \frac{G_{LT} t_w^3}{12} = \frac{(590,000)(0.3)^3}{12} = 1,328 \ lb\text{-}in$$

$$(\sigma_{ss}^{ss})_w = \left(\frac{\pi^2}{(0.3)(2(4.562))^2}\right)\left(13.9\sqrt{(7,145)^2} + 11.1(2,358) + 22.2(1,328)\right) = 61,252 \ psi$$

If the ratio of the flange simply-supported buckling stress to flange longitudinal compressive modulus is less than the ratio of the web simply-supported buckling stress to web longitudinal compressive modulus, then the flange buckles first. For the prototype FRP deck section,

$$\frac{(\sigma_{ss}^{ss})_f}{(E_L)_f} = \frac{46,030}{2,304,000} = 0.01998$$

$$\frac{(\sigma_{ss}^{ss})_w}{(E_L)_w} = \frac{61,252}{2,830,000} = 0.02164$$

Therefore, the flange buckles first, which is consistent with the full scale flexural test results. The next step would be to determine the degree of restraint provided by the web and revise the buckling stress for the flange. However, an initial check of the required moment to buckle the flange even with the lower bound stress results in a value much higher than the peak test result from **Table 6.2**, namely,

$$M = (\sigma_{ss}^{ss})_f \frac{I_x}{y} = (46.03)\left(\frac{753.0}{(9.25/2)}\right) = 7,494 \ in\text{-}k > 2,785 \ in\text{-}k$$

However, visual observations during the test indicated that the flange did not buckle only between the two outermost webs, which is the basis for Equation 6.5. Instead, the flange buckled as if there was only minimal bracing provided by the outermost web, as shown in **Figure 6.2**. The buckling mode resembled that of a flange for an I-shaped cross section, with the innermost edge supported by the web and the outermost edge free. As a result, the research team examined the buckling equations for a flange with one longitudinal edge simply supported and the other free to deform, Equation 6.7.

$$(\sigma_{free}^{ss})_f = \frac{4t_f^2}{b_f^2} G_{LT} \tag{6.7}$$

For the flange of the prototype FRP deck section,

$$(\sigma_{free}^{ss})_f = \frac{4(0.49)^2}{(7.845)^2}(720,000) = 11,235 \ psi$$

As this buckling stress is less than the previous value, flange buckling still controls over web buckling, and the next step involves determining the degree of elastic restraint provided to the flange by the web. In this case, this restraint is provided by the first interior web due to

debonding along the outermost web. The equations for the buckling stress of a flange, σ_{cr}^{local}, accounting for the degree of restraint provided by the web and having the other longitudinal edge free to deform are shown as Equations 6.8 through 6.10.

$$\sigma_{cr}^{local} = \frac{1}{(b_f/2)^2 t_f} \left(7 \sqrt{\frac{D_L D_T}{1 + 4.12 \zeta_{I-flange}}} + 12 D_s \right) \tag{6.8}$$

$$\zeta_{I-flange} = \frac{(D_T)_f}{k_{I-flange} L_T} \tag{6.9}$$

$$k_{I-flange} = \frac{2(D_T)_w}{d_w} \left(1 - \frac{(\sigma_{free}^{ss})_f (E_L)_w}{(\sigma_{ss}^{ss})_w (E_L)_f} \right) \tag{6.10}$$

For the flange of the prototype FRP deck section assuming a loss of elastic restraint from the outermost web,

$$k_{I-flange} = \frac{2(7,145)}{(2(4.562))} \left(1 - \frac{(11,235)(2,830,000)}{(61,252)(2,304,000)} \right) = 1,213 \; lb$$

$$\zeta_{I-flange} = \frac{25,349}{(1,213)(7.845)} = 2.664$$

$$\sigma_{cr}^{local} = \frac{1}{(7.845/2)^2 (0.49)} \left(7 \sqrt{\frac{(25,349)^2}{1 + 4.12(2.664)}} + 12(7,059) \right) = 18,042 \; psi$$

and the moment to cause buckling of the flange (top facesheet) is calculated as

$$M = (\sigma_{cr}^{local}) \frac{I_x}{y} = (18.04) \left(\frac{753.0}{(9.25/2)} \right) = 2,937 \; in\text{-}k \cong 2,785 \; in\text{-}k$$

which is approximately equal to the peak force effect from **Table 6.2**.

The lack of elastic restraint provided by the outermost web may have been due to transverse bending stresses generated in the vicinity of the concentrated load or some type of inherent defect between the web laminates and the flange laminates. In any event, it is important to note that the final version of the prototype FRP deck for an actual bridge would include end closures, such as those used for the panel-to-panel connection tests (Section 4), which would reinforce against this buckling failure mode. However, even without those improvements, the prototype FRP deck panel supported an average failure load nearly three times the AASHTO Design Truck factored wheel load, 108.2 kips versus 37.2 kips (Section 3), indicating a level of safety for these panels far beyond that required by code.

Figure 6.2: Local Buckling of Compression Flange, Specimen FP-1

6.4. LOCAL BUCKLING OF THE WEBS DUE TO IN-PLANE SHEAR

The webs of an FRP profile can buckle in shear at locations of high shear forces, either near supports or at locations of concentrated loads. The equation for the buckling of an orthotropic plate in pure shear is a function of the restraint provided by the flanges, the aspect ratio, and the orthotropy ratio (E_L/E_T). The critical shear stress for local shear buckling of an orthotropic plate is calculated using Equations 6.11 through 6.13.

$$\tau_{cr}^{local} = \frac{4k_{LT}\sqrt[4]{D_L D_T^3}}{t_w d_w^2} \tag{6.11}$$

$$k_{LT} = 8.125 + 5.045K \tag{6.12}$$

$$K = \frac{2D_s + D_{LT}}{\sqrt{D_L D_T}} \tag{6.13}$$

For the web of the prototype FRP deck section,

$$K = \frac{2(1,328) + 2,358}{\sqrt{(7,145)^2}} = 0.7017$$

$$k_{LT} = 8.125 + 5.045(0.7017) = 11.665$$

$$\tau_{cr}^{local} = \frac{4(11.665)\sqrt[4]{(7,145)^4}}{(0.3)(2(4.562)^2)} = 13,349 \; psi$$

and the critical shear force to cause local shear buckling of the webs is calculated as

$$V_{cr}^{local} = \tau_{cr}^{local} \frac{I_x t}{Q} \cong \tau_{cr}^{local} A_{web}$$

$$V_{cr}^{local} = (13.35)[(6\ webs)(0.3)(2(4.562))] = 219.2\ kips$$

which is much greater than the peak force effect from **Table 6.2**, which is consistent with the fact that the web did not experience a shear buckling failure during the tests. However, as noted previously, the combined shear and bearing test indicated failure by excessive bearing stresses beneath the concentrated load prior to a shear failure, and, as a result, there is no peak shear failure load to compare with the result of the design equation.

6.5. LOCAL CRUSHING OR BUCKLING OF THE WEBS DUE TO CONCENTRATED LOADS

The webs of an FRP profile can fail due to local crushing or buckling at locations of concentrated loads, either near supports or along the span. The critical web crushing stress is assumed to be equal to the transverse compressive strength of the web material, with the stress acting over an effective length of the web equal to the load length plus the web depth, as shown in Equations 6.14 and 6.15.

$$(\sigma_y)_{cr}^{crush} = \sigma_{T,c} \tag{6.14}$$

$$F_{cr}^{crush} = (\sigma_y)_{cr}^{crush} A_{eff} \tag{6.15}$$

The web may also buckle in the vertical plane as if it were a wide, slender column. In this case, it is assumed that the web acts as a plate simply supported along its loaded edges (parallel to the load direction) with the load applied over an effective length of the web equal to the load length plus the web depth, as shown in Equations 6.16 and 6.17.

$$(\sigma_y)_{cr}^{local} = \left(\frac{2\pi^2}{t_w l_w^2}\right)\left(\sqrt{D_L D_T} + D_{LT} + 2D_S\right) \tag{6.16}$$

$$F_{cr}^{local} = (\sigma_y)_{cr}^{local} A_{eff} \tag{6.17}$$

For the web of the prototype FRP deck section,

$$(\sigma_y)_{cr}^{crush} = 64.6\ ksi$$

$$(\sigma_y)_{cr}^{local} = \left(\frac{2\pi^2}{(0.3)(9.842)^2}\right)\left(\sqrt{(7,145)^2} + 2,358 + 2(1,328)\right) = 8,259\ psi = 8.26\ ksi$$

which indicates that local web buckling due to the concentrated load governs over local web crushing, and the critical transverse load is calculated as

$$F_{cr}^{local} = (8.26)[(2\ webs)(0.3)(20 + 2(4.562)] = 144.4\ kips \cong 134.9\ kips$$

which is approximately equal to the peak force effect from **Table 6.2**, and is consistent with the fact that the webs buckled immediately beneath the concentrated load during the tests, as shown in **Figure 6.3**.
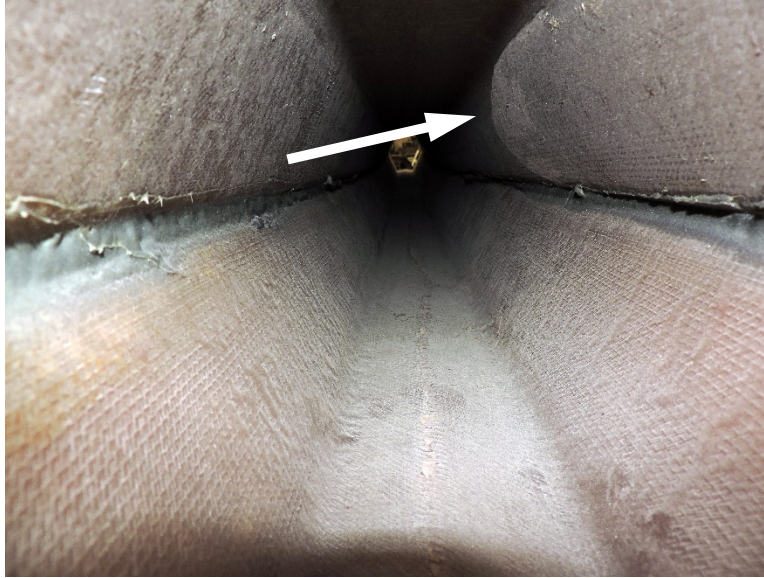
Figure 6.3: Buckling of Upper Right Sloping Web Located Below Load Point

6.6. SUMMARY

It appears that existing FRP design equations can reasonably predict the response and behavior of the VARTM-manufactured, prototype FRP bridge deck panels. The equations correctly predicted a flexural failure due to local buckling of the compression flange and a bearing failure due to local buckling of the webs beneath the concentrated load. Not only was the mode of failure predicted correctly, but the forces that initiated failure were within 7% of the design equation values, 2,785 in-k peak test value versus 2,937 in-k capacity for a flexural failure and 134.9 kip peak test value versus 144.4 kip capacity for the bearing failure. All other potential modes of failure – strength material failures, web buckling due to flexural stresses, and web buckling due to in-plane shear – had capacities that well exceeded the peak design forces, which is consistent with observations during the full scale testing.

7. FRP BRIDGE DECK OVERLAY

The FRP deck requires an overlay to both protect the top facesheets of the panels and to provide a wearing/traction surface for vehicular traffic. The research team investigated both cementitious and non-cementitious-based materials for the overlay. The investigation included ease of application, bond strength to the FRP, and the effects of temperature and shrinkage on the behavior of the composite system. The following section discusses the different types of overlay materials, development of a latex modified concrete overlay option, fabrication of the FRP/overlay specimens, details of the environmental exposure protocol, and results of the bond testing.

7.1. GENERAL

The research team investigated three different types of potential overlays for the FRP deck: latex modified concrete, polymer concrete, and a hybrid system. Latex modified concrete (LMC) is a portland cement concrete in which an admixture of latex emulsion is used to replace a portion of the mixing water. Polymer concretes use a polymer binder, such as epoxies, polyesters, and methacrylate, in place of portland cement. The hybrid system consisted of an initial layer of polymer concrete bonded to the FRP followed by a layer of LMC.

LMC has traditionally been used as an overlay for existing reinforced concrete bridge decks, with thicknesses ranging from 1 to 2 inches. Polymer concrete overlays, on the other hand, are usually much thinner, ranging from 1/4 to 1/2 inches in thickness. The benefits of LMC include low permeability and improved freeze-thaw resistance, compressive strength, tensile strength, and bond strength compared to traditional portland cement concrete. The benefits of polymer concrete include extremely low permeability and very high compressive strength, tensile strength, and bond strength compared to traditional portland cement concrete.

In order to evaluate the bond strength and compatibility between the different overlay options and the FRP bridge deck, the research team fabricated four (4) FRP facesheet specimens. The facesheets, shown in **Figure 7.1**, measure 4 ft. x 5 ft. in plan with a 1/2 in. thickness. Each facesheet has an identical fiberglass/resin construction as the top facesheet of the full scale, prototype FRP deck panels. One side of the specimens contained a polyester mat embedded in the resin for enhanced bonding to the overlay materials, while the opposite side represented a plain resin surface. Initially, the research team considered investigating both the polyester mat surface and the plain resin surface for bonding with the overlay materials, but preliminary tests indicated far superior performance with the embedded polyester mat.

7.2. LATEX MODIFIED CONCRETE OVERLAY DEVELOPMENT

The research team developed a latex modified concrete (LMC) mix design as a potential overlay material. The mix development involved a study of several different types of additives, in addition to the latex, in order to improve performance. These additives were aimed at reducing shrinkage in the overlay material to prevent cracking and potential debonding. Target performance values for the LMC overlay consisted of the following:

- Slump: 5 to 9 in. (can be varied for ease of placement of the overlay)
- Air Content: 4% to 7%
- Compressive Strength at 28 days ≥ 3,500 psi
- Bond Strength to FRP Deck ≥ 250 psi

All overlay mixtures were made with well-graded natural river sand and crushed limestone aggregate with a maximum size aggregate (MSA) of 3/8 in. Specific gravity values of the sand and coarse aggregate were 2.6 and 2.5, respectively. In total, four optimized latex modified concretes were prepared, as summarized in **Table 7.1**.
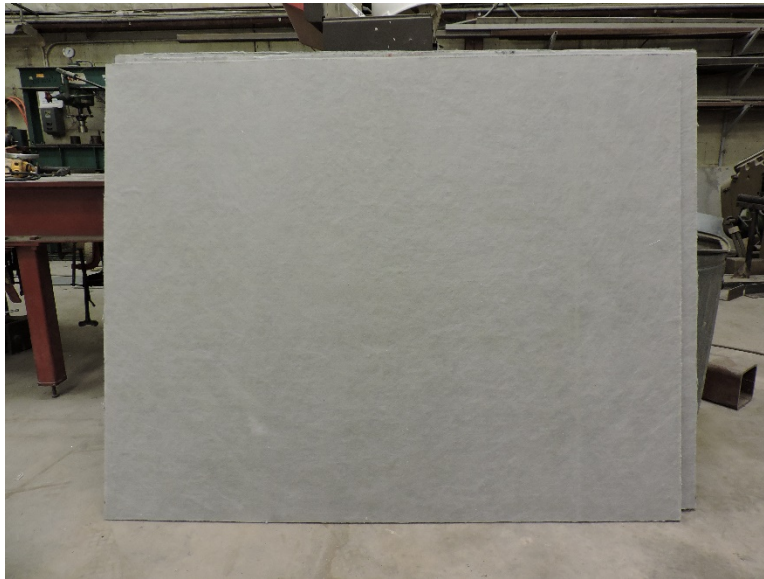
Figure 7.1: FRP Facesheet Specimens for Overlay Testing

The reference latex-modified concrete (LMC-100C) was made with 100% Type I/II cement. The LMC-15K, LMC-5PC, LMC-2CRA mixtures were prepared with 15% Type K expansive agent (KSC Komponent), 5% MgO-based expansive agent (Premier Prevent-C), and 2% crack-reducing admixture (CRA from BASF), by mass of total binder, respectively. For all the mixtures, 30 minutes of mixing time for the latex (Styrofan 1186) and coarse aggregate was applied before introducing cement and sand.

All the mixtures that were proportioned with the same w/cm of 0.39 exhibited similar slump of 8 to 9 in. and air content of 5% to 6%. No water-reducing admixture and air-entraining admixture was needed in most of the optimized mixtures since the incorporation of latex was sufficient to meet these requirements. The LMC-2CRA mixture had relatively low air content compared to those of the other mixtures. Use of air-entraining admixture may be needed for the LMC-2CRA mixture or an increase in mixing time with the latex (Styrofan 1186) and coarse aggregate is required to entrain more air volume. Regardless of the type of expansive agent and

CRA, all three mixtures were very stable and had high workability which can facilitate the placement of a thin overlay over the FRP deck panel.

Table 7.1: Composition and Properties of LMC Mixtures

	LMC No. 1 (Reference)	LMC No. 2	LMC No. 3	LMC No. 4
Codification	LMC-100C	LMC-15K	LMC-5PC	LMC-2CRA
Cement (Type I/II) (lb/yd^3)	657	560	624	657
Komponent (lb/yd^3), Type K expansive agent	-	98 (15% by mass)	-	-
Prevent C (lb/yd^3), MgO-based expansive agent	-	-	34 (5% by mass)	-
Crack-reducing admixture (% by mass of binder)	-	-	-	2
Latex, Styrofan 1186 (lb/yd^3)*	209	209	209	209
Batch water (lb/yd^3)**	143	143	143	130
w/p or w/cm	0.39	0.39	0.39	0.39
Sand (lb/yd^3)	1466	1463	1460	1466
Coarse aggregate (lb/yd^3)	1197	1193	1193	1197
S/A by mass	0.55	0.55	0.55	0.55
Slump (in.)	9	8	8	8.5
Air content (%)	5.0	6.0	5.0	**3.5**
Temperature (°F)	68.5	69.8	68.7	69.1
Initial setting time (hr)	7.5	4.8	6.4	8.1
Final setting time (hr)	9.5	6.5	8.1	10.7
7-d compressive strength (psi)***	4,205	3,175	4,395	3,815
28-d compressive strength (psi)	5,860	5,295	5,875	5,035
56-d compressive strength (psi)	6,455	6,220	6,945	5,890

* 15% solid mass by mass of cement (solid content of latex = 48%)

** Batch water was decreased by the amount of liquid in CRA and Latex.

*** 2 days of moist curing then air drying until the age of testing.

All the LMC mixtures exhibited 28-day compressive strengths higher than the minimum requirement, 3,500 psi. Mixtures made with15% Type K expansive agent (LMC-15K) and 5% MgO-based expansive agent (LMC-5PC) had compressive strengths similar or greater than the reference mix, which had 100% Type I/II cement. The LMC-2CRA mixture containing 2% CRA had 9% to 15% lower compressive strengths than those of the reference mix.

All cast cylinders and prisms for total shrinkage were moist cured for 2 days, then were subjected to air-drying at $73 \pm 2°F$ and $50 \pm 5\%$ R.H. The curing regime is typical for the LMC. Autogenous shrinkage was monitored from the time of final setting. On the other hand, total shrinkage measurement started after demolding at 1 day.

Autogenous and total shrinkage results are presented in **Figures 7.2** and **7.3**, respectively. Autogenous shrinkage is measured from time of final setting. Drying shrinkage is measured starting at one day after casting, with a curing regime of two days of moist cure followed by air drying. The LMC-15K made with 15% Type K expansive agent exhibited significantly greater expansion than the other mixtures under sealed conditions, as presented in **Figure 7.2**. It is very important to note that the expansion of the LMC-15K mixtures continued up to approximately 20 days of age, which can lead to significant reduction of the risk of cracking at early ages. The LMC-CRA mixture exhibited lower autogenous shrinkage compared to those made with 5% MgO-based expansive agent and 100% cement.

The three LMC mixtures containing expansive agents and CRA exhibited similar drying shrinkage characteristics, regardless of the type of expansive agent or use of shrinkage-reducing admixture, as shown in **Figure 7.3**. The drying shrinkage values of these mixtures were 40% to 55% lower than that of the reference mix.

Based on the results of the fresh properties, compressive strength, autogenous shrinkage, and drying shrinkage, the LMC-15K containing 15% Type K expansive agent was selected to move forward to the next stage. This mixture will be used for further investigation of bond strength and compatibility between the overlay and FRP panel.

7.3. FRP/OVERLAY SPECIMEN PREPARATION

The research team investigated several potential polymer concrete overlay options and settled on two from Transpo Industries, Inc., and one from Euclid Chemical. Combined with the LMC mix design discussed in Section 7.2, a total of five (5) overlay options underwent further testing. These consist of the following:

- T-48 polysulfide epoxy overlay (Transpo Industries, Inc.)
- T-18 methyl methacrylate (MMA) overlay (Transpo Industries, Inc.)
- Flexolith low modulus epoxy overlay (Euclid Chemical)
- Latex modified concrete overlay LMC-15K (Section 7.2)
- Hybrid overlay with polymer concrete initial layer followed by LMC-15K layer

The overlay thicknesses were set at 1/4 in. for the polymer concretes and 1-1/2 in. for the LMC, with the polymer concrete overlay thickness selected based on recommendations from the
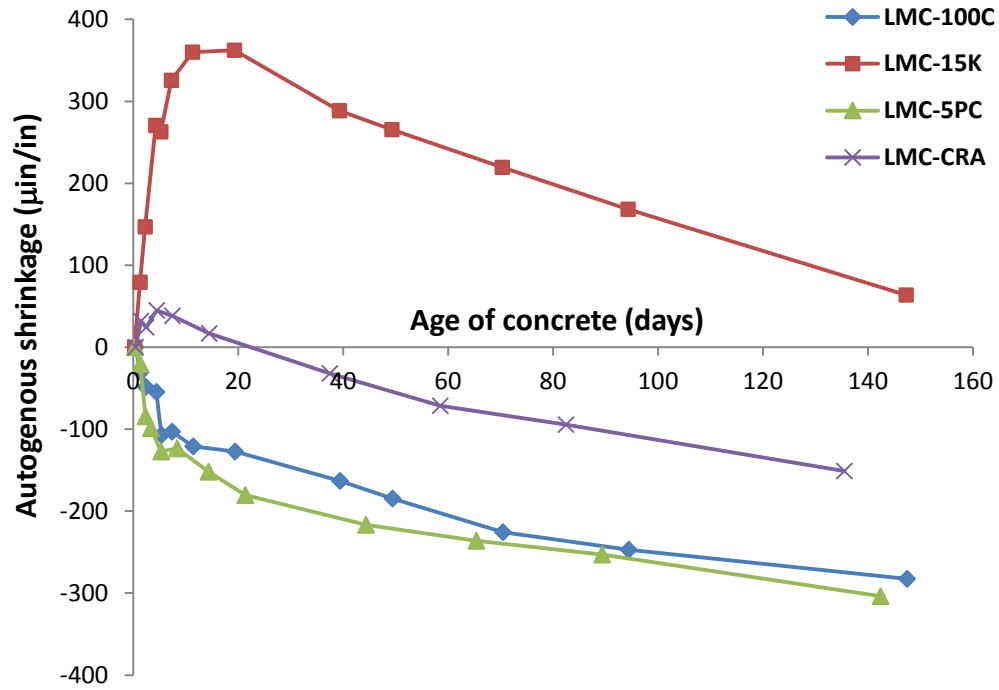
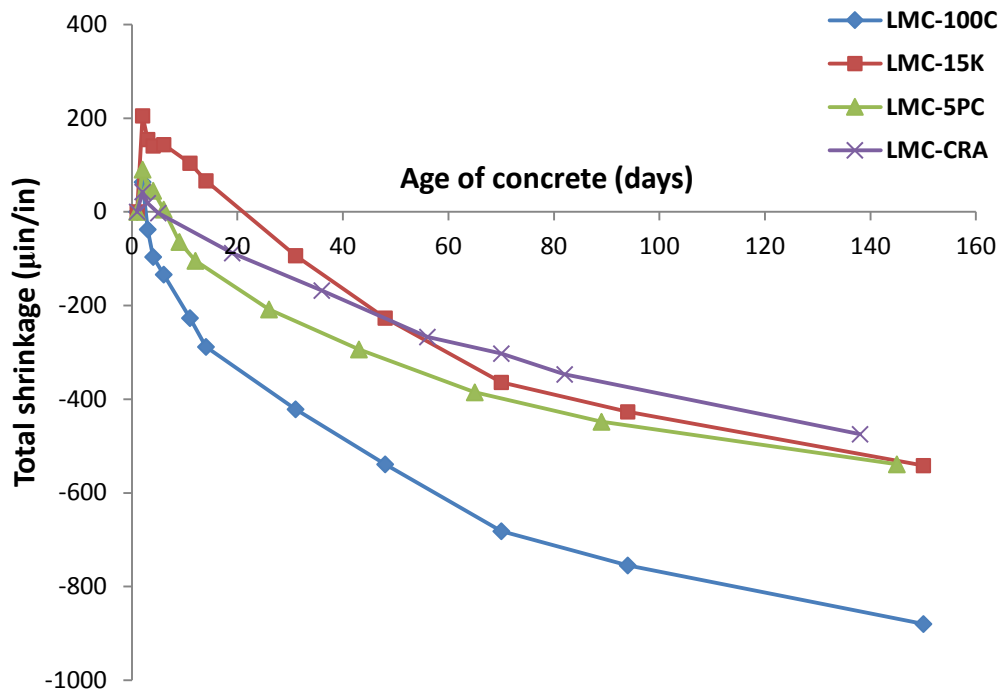**Figure 7.2: Autogenous Shrinkage with Respect to Time**

Figure 7.3: Drying Shrinkage with Respect to Time

manufacturers, and the LMC overlay thickness selected based on experience of the research team with traditional overlay repairs of concrete bridge decks. The hybrid system consisted of a total thickness of 1-1/2 in., with a 1/4-in.-thick polymer concrete layer adjacent to the FRP overlaid with a 1-1/4-in.-thick LMC layer.

The top facesheet specimens, **Figure 7.1**, were sectioned into 1 ft. x 1 ft. segments in order to prepare several FRP/overlay samples for bond and compatibility testing. Due to the presence of the embedded polyester mat, special precautions were required to section the panels without damaging the mat. However, it is important to note that special precautions would not be required on an actual bridge deck as the panels would be fabricated to the correct sizes. After considering several options, the research team settled on high pressure waterjet cutting to section the panels. For the polymer concrete overlays, five (5) samples were prepared, with four (4) used to test the polymer concrete overlay and the fifth sample used to prepare a hybrid overlay option. Four (4) samples were prepared for the LMC overlay. The sectioned FRP facesheet specimens were inserted into molds for casting the overlay materials, as shown in **Figure 7.4**.
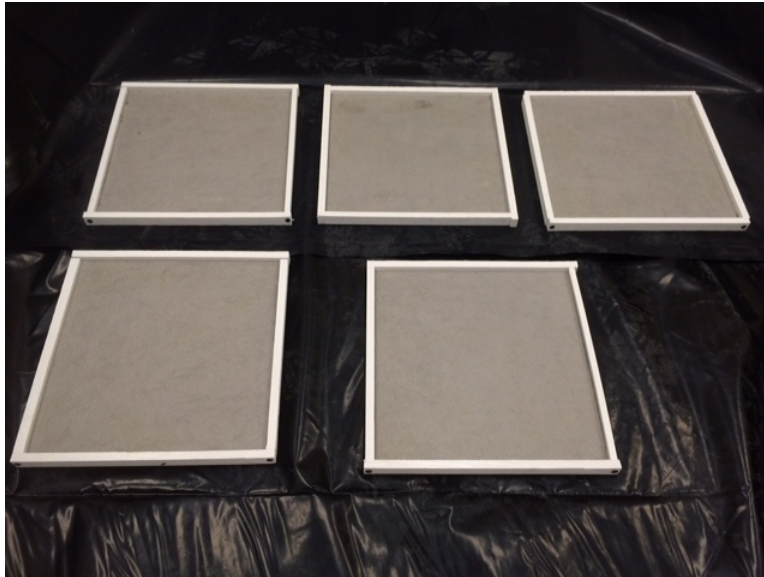

Figure 7.4: FRP Facesheet Specimens Prepared for Overlay Casting

All of the overlay materials were prepared in accordance with the mixing proportions and recommendations of each material supplier. Details of each are discussed in the following subsections of the report.

7.3.1. T-48 Polysulfide Epoxy Overlay. A primer consisting of components A (resin) and B (hardener) were mixed at a 2:1 volume proportion and applied thoroughly to the polyester mat using a roller. Before the primer dried, the same resin and hardener were thoroughly mixed in the same proportions as the primer before introducing the T-48 powder component. After 2 minutes of mixing the three components, the overlay material was poured directly on top of the

primed surface of the FRP panel, as shown in **Figure 7.5**. After 20 minutes, flint rocks were broadcast on the overlaid surface to improve skid resistance (**Figure 7.6**).
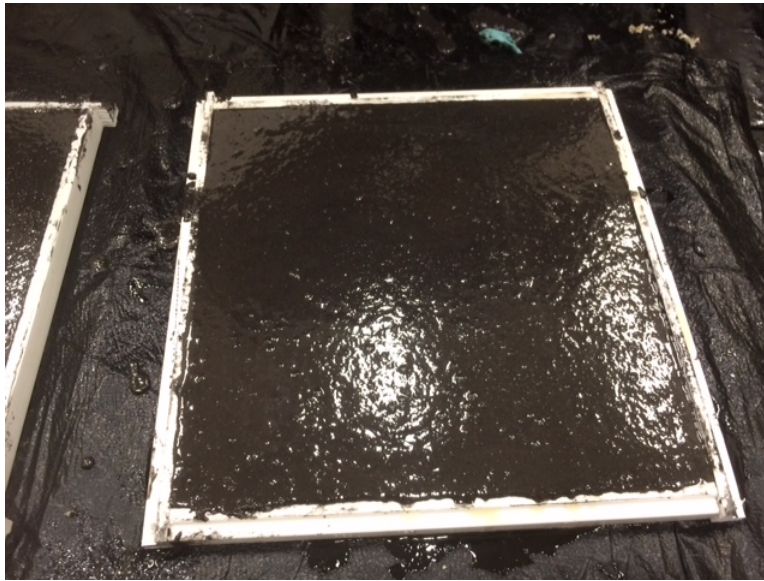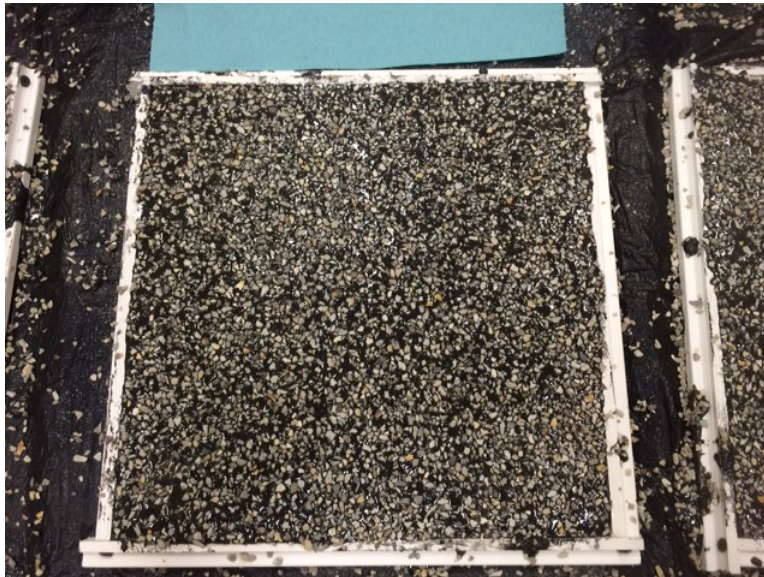

Figure 7.5: T-48 Slurry Applied to Segment of FRP

Figure 7.6: T-48 Overlay After Broadcasting of Flint Rocks

7.3.2. T-18 Methyl Methacrylate (MMA) Overlay. One liter of T-18 primer and 30 g of powder hardener were mixed and applied thoroughly to the polyester mat surface of the FRP panel. A silica sand was then broadcast on the primed surface for improved bonding between the panel and overlay materials. Before the primer dried, the T-18 resin was thoroughly mixed with the powder hardener before introducing the T-18 powder component. After 60 seconds of mixing the three components, the overlay material was poured directly on top of the primed surface of the FRP panel. The same flint rocks were broadcast on the overlaid surface (**Figure 7.7**). After 1 hour, excess flint rocks were removed with a broom, and the T-18 topcoat was applied using a roller, as shown in **Figure 7.8**.

7.3.3. Flexolith Low Modulus Epoxy Overlay. A primer consisting of the A and B resins was mixed at a 1:1 volume proportion and applied thoroughly to the polyester mat surface of the FRP panel. Before the primer dried, the A and B resins were again mixed in the same proportions as the primer. However, after mixing the resins for 3 minutes, unlike the other polymer concrete overlays, the flint rocks were mixed directly with the epoxy resin. Once the flint rocks were thoroughly mixed, the prepared Flexolith was poured directly on top of the primed surface of the FRP panel, as shown in **Figure 7.9**.

7.3.4. Latex Modified Concrete and Hybrid Overlays. The LMC-15K mix design selected to proceed to the next stage of testing (Section 7.2) was thoroughly mixed following standard concrete mixing operations. The material was then poured either directly onto the polyester mat surface of the FRP for the LMC overlay option or directly onto the previously placed polymer concrete overlays for the hybrid overlay option. A prepared specimen of the LMC overlay is shown in **Figure 7.10**.
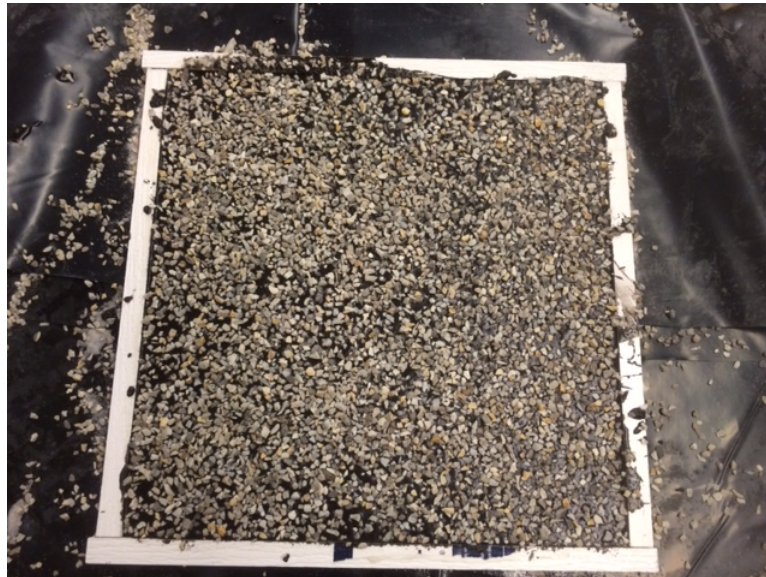

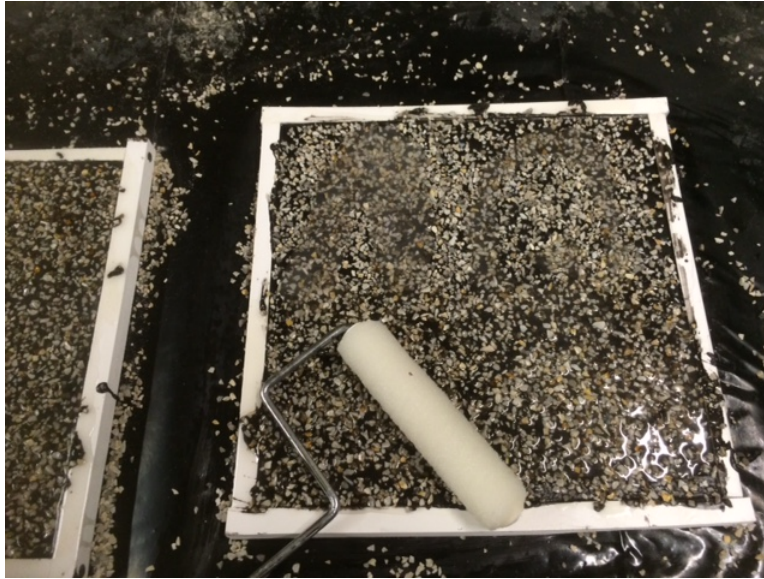**Figure 7.7: T-18 Overlay After Broadcasting of Flint Rocks**

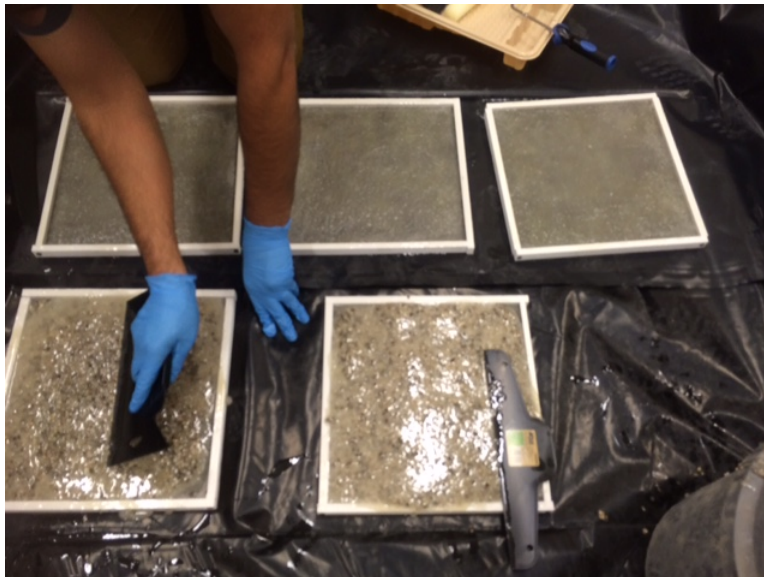**Figure 7.8: T-18 Overlay Topcoat Application**

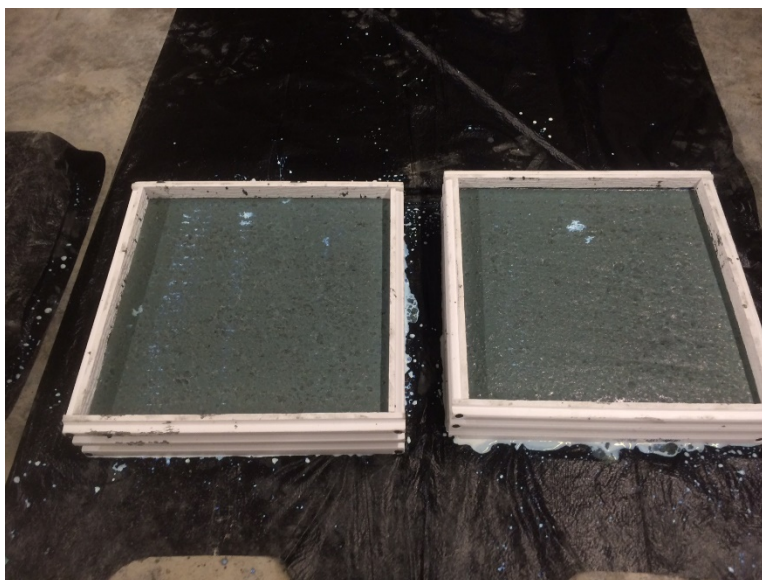**Figure 7.9: Placement of Flexolith Overlay Material**

Figure 7.10: Latex Modified Concrete Overlay

7.4. BOND STRENGTH/THERMAL COMPATIBILITY STUDY

Two of the most important characteristics of potential overlay materials involves bond strength and thermal compatibility with the FRP. The research team developed a series of environmental exposures of the FRP/Overlay specimens. Details of the exposure conditions are shown in **Table 7.2**. Exposure Series I was based on ASTM C672, a standard test method for freeze-thaw scaling resistance. Exposure Series II was based on ASTM C884, a standard test method for thermal compatibility between concrete and an epoxy-resin overlay. Condition 1 of Series II follows the ASTM standard, while Condition 2 of Series II adds a high temperature exposure to mimic an actual bridge deck. Optional Condition 3 of Series II included submerging the samples in water for 24 hours followed by the ASTM C884 protocol.

Except for a control set of specimens, all of the FRP/overlay samples underwent exposure to the environmental conditions detailed in **Table 7.2**. After each exposure, the samples were thoroughly inspected for any signs of debonding or delamination. Also after each exposure, one of the samples for each FRP/overlay system underwent direct pull-off bond testing, as shown in **Figure 7.11**. In addition to evaluating bond strength, the pull-off testing completed after each exposure cycle provided an indirect means of assessing compatibility between the FRP deck and the overlay. Incompatibility between the two materials would result in partial or complete debonding due to the thermal cycling, which would degrade the bond strength.

Inspection of the samples after completion of exposure Series I revealed that the Flexolith-LMC hybrid overlay debonded between the two materials for all of the specimens, as shown in **Figure 7.12**. This result is most likely due to the finish topcoat used as part of the Flexolith overlay system. All of the other samples did not reveal any signs of debonding.

Table 7.2: Details of Environmental Exposure Conditions to Investigate Bond Strength and Thermal Compatibility

Exposure Series I (ASTM C672, 21 of cycles)			Exposure Series II		
Time (hr)	Temperature (°F)	Chamber	Type	Detail	Chamber
0	77		Condition 1 (ASTM C884)	5 cycles of (total 10 days): • 77°F for 24 hrs • -10°F for 24 hrs	
8	0		Condition 2	5 cycles of (total 15 days): • -10°F for 24 hrs • 77°F for 24 hrs • 140°F for 24 hrs	
16	0				
22	77		Condition 3 (**optional**)	5 cycles of (total 15 days): • Submerging in water for 24 hrs • -10°F for 24 hrs • 77°F for 24 hrs	
24	77				

Figure 7.11: Direct Pull-off Bond Testing of Overlay Materials
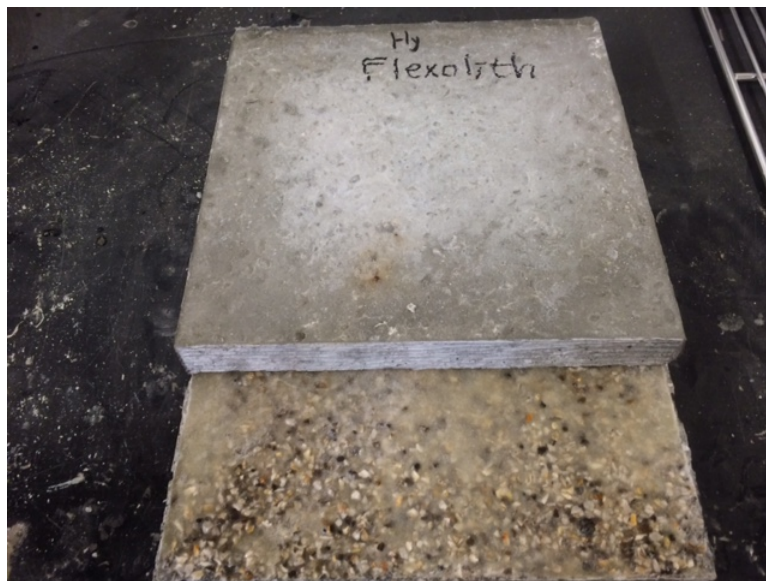
Figure 7.12: Debonding Between Flexolith and LMC in Hybrid Overlay System

Bond strength test results for the FRP/overlay samples are summarized in **Table 7.3** and **Figure 7.13**. Except for the Flexolith-LMC hybrid overlay, all of the other overlay samples completed the full range of environmental cycles without any signs of debonding or delamination. In general, the epoxy-based overlay materials exhibited significantly higher bond strengths compared to the T-18 and LMC overlays. The T-48 and Flexolith overlays had bond strength values between 206 and 286 psi compared to values between 55 and 113 for the T-18 overlay and between 57 and 86 for the LMC overlay.

It is also important to note that the epoxy-based materials exhibited consistent bond strength with respect to the different environmental exposure cycles. In particular, the Flexolith overlay had no reduction in the bond strength for successive exposures and, in fact, exhibited a slight increase. For the T-18 overlay, the material failed within the overlay and, as a result, the bond strength between the overlay and FRP panel could not be determined. Bond strengths for the LMC overlays decreased for successive exposure cycles.

Regardless of the overlay materials, the hybrid overlays exhibited lower bond strengths than the epoxy-based overlays. In fact, all of the hybrid overlay systems failed at the interface between the polymer concrete and the LMC, as shown in **Figure 7.14** for the T-48/LMC hybrid and in **Figure 7.15** for the T-18/LMC hybrid. The Flexolith/LMC hybrid debonded after exposure Series I.

Based on the bond strengths before and after the exposure cycles, the T-48 and Flexolith overlay materials outperformed the other potential overlays. Both materials developed a high chemical bond with the FRP facesheet and showed excellent thermal compatibility throughout the environmental protocol. The hybrid systems are not recommended as potential candidates for an actual bridge deck

7.5. SUMMARY

The epoxy-based overlay materials developed exceptional bonding to the FRP facesheet and revealed excellent compatibility with the substrate throughout the environmental exposure cycles. Both the T-48 and Flexolith overlays are recommended as potential candidates for an actual bridge deck. The methyl methacrylate overlay had slightly higher bond strengths than the optimized latex modified concrete overlay. Neither system is recommended as a potential overlay for the FRP deck.

Table 7.3: Direct Pull-off Bond Strength Test Results

| Overlay | Sample | Reference | | Series I | | Series II | | | |
| | | No exposure | | ASTM C672 | | (-)10 and 77 ºF cycle | | (-)10, 77, and 140 ºF cycle | |
		Pull-off strength (psi)	Failure mode	Pull-off strength (psi)	Failure mode	Pull-off strength (psi)	Failure mode	Pull-off strength (psi)	Failure mode
LMC	1	70	bond	88	bond	66	bond	52	bond
	2	90	bond	44	bond	75	bond	72	bond
	3	110	bond	61	bond	74	bond	61	bond
	4	72	bond	87	bond	74	bond	44	bond
	mean	86		70		72		57	
T-48	1	251	bond	219	bond	190	bond	276	bond
	2	220	bond	225	bond	225	bond	233	bond
	3	208	bond	243	bond	232	bond	211	bond
	4	276	bond	241	bond	177	bond	243	bond
	mean	239		232		206		241	
T-18	1	110	overlay	53	overlay	68	overlay	61	overlay
	2	101	overlay	40	overlay	74	overlay	74	overlay
	3	125	overlay	66	overlay	85	overlay	56	overlay
	4	115	overlay	59	overlay	68	overlay	64	overlay
	mean	113		55		74		64	
Flexolith	1	199	bond	243	bond	281	bond	331	bond
	2	247	bond	201	bond	197	bond	266	bond
	3	247	bond	272	bond	269	bond	288	bond
	4	198	bond	269	bond	283	bond	258	bond
	mean	222		246		257		327	

Table 7.3 (cont'd): Direct Pull-off Bond Strength Test Results

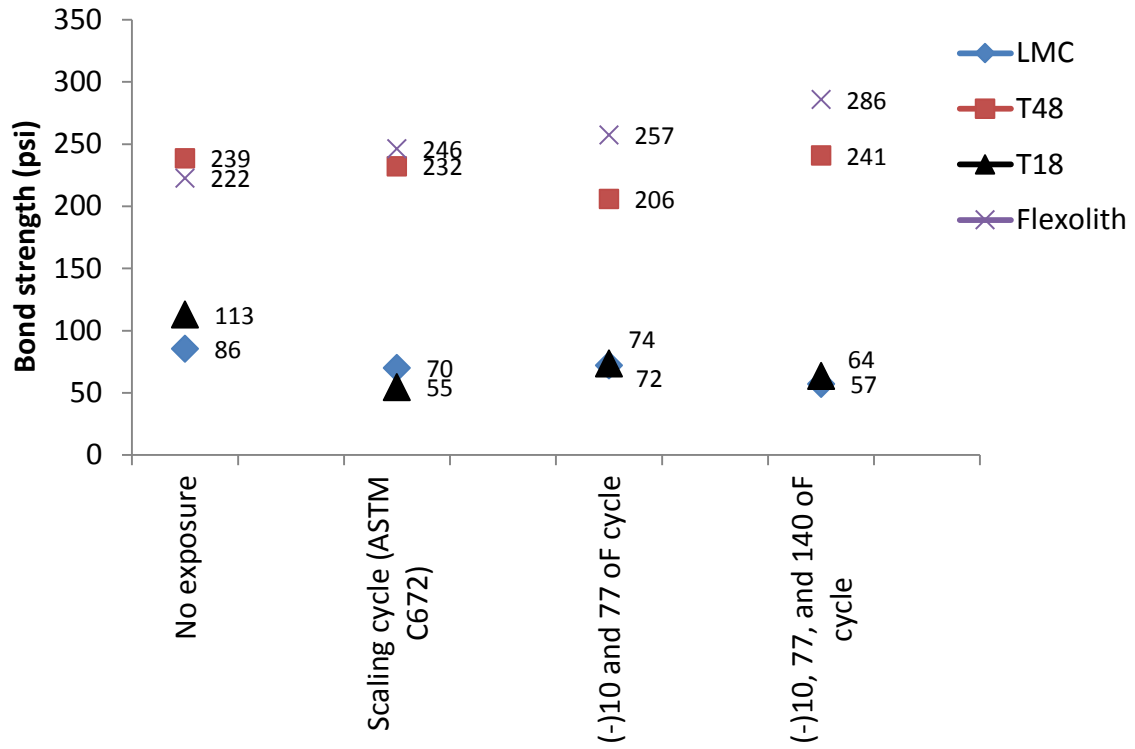|		Reference		Series I				Series II	
		No exposure		ASTM C672		(-)10 and 77 ºF cycle		(-)10, 77, and 140 ºF cycle	
Overlay	Sample	Pull-off strength (psi)	Failure mode	Pull-off strength (psi)	Failure mode	Pull-off strength (psi)	Failure mode	Pull-off strength (psi)	Failure mode
T-48 hybrid	1							136	T-48/LMC
	2							135	T-48/LMC
	3							120	T-48/LMC
	4							147	T-48/LMC
	mean							135	
T-18 hybrid	1							61	T-18/LMC
	2							84	T-18/LMC
	3							99	T-18/LMC
	4							101	T-18/LMC
	mean							86	
Flexolith hybrid	1	Debonded between Flexolith and LMC after exposure							
	2								
	3								
	4								
	mean								

Figure 7.13: Direct Pull-off Bond Strength Test Results

Figure 7.14: Bond Failure at Interface of T-48 and LMC

Figure 7.15: Bond Failure at Interface of T-18 and LMC

8. ADDITIONAL DESIGN ISSUES

The research team also investigated several other design issues necessary to fully evaluate the ability to implement the prototype FRP deck panels on an actual bridge. These issues included the panel-to-girder connection, skewed bridges, drainage, and anticipated costs relative to traditional cast-in-place reinforced concrete decks. The following section discusses these issues.

8.1. PANEL-TO-GIRDER CONNECTION

The research team investigated both mechanical and bonded methods of attaching the panels to the bridge girders. Based on previous studies on FRP bridge decks, there is conflicting data on whether either method leads to composite action with the girders, and the majority of the field implementation studies did not design the deck to support the compressive or tensile stresses from composite action. The two most important reasons for providing a positive connection between the panels and girders is to provide lateral bracing of the girders and to resist horizontal forces due to traffic, such as centrifugal, skidding, and wind loads.

The methyl methacrylate (MMA) adhesive used to form the deck panel (Section 2) and provide the bonded panel-to-panel connection (Section 4) has several advantages that make it a viable candidate for a bonded panel-to-girder connection. The cure profile of MMA adhesives can be adjusted to allow more time for adhesive application and assembly of parts, which would allow sufficient time to place and adjust sections of the deck prior to hardening of the joint. Furthermore, less surface preparation is required for MMA adhesives compared to epoxies and polyurethanes. A bonded joint would also eliminate the need for any special pockets, inserts, or hardware to connect the panels to the girders.

The research team also investigated several mechanical methods for connecting the panels to the girders. The method that showed the greatest promise involved forming a pocket in the deck to allow installation of headed shear studs to the steel girders. Headed shear studs have traditionally been installed on bridge girders to provide a positive connection and composite action with cast-in-place concrete decks. Once the deck panels are positioned, the pockets would be grouted to provide the mechanical connection between the panels and girders. The pocket should extend a minimum distance of 6 in. longitudinally each side of the studs and can be formed with foam dam inserts. The grout (or mortar) should have a minimum flow table spread of 9 in. An example is shown in **Figures 8.1** and **8.2** for the prototype FRP deck panels. In the case of precast concrete girders, reinforcing bars cast with the girders would substitute for the headed shear studs.

8.2. BRIDGE SKEW

A skewed bridge requires modification to the prefabricated FRP deck panels. There are two options for fabricating the panels to provide the deck for a skewed bridge. Option 1 involves fabricating skewed panels to accommodate the shape of the bridge deck, as shown in **Figure 8.3**. These parallelogram-shaped panels are easily fabricated with little waste by sectioning very long

runs of the panel. All of the panels would be identical. The only downside of this approach is that the effective span of the panels is slightly longer because of the skew shape. Option 2 involves fabricating standard rectangular-shaped panels for the majority of the deck and using non-standard end panels to complete the deck, as shown in **Figure 8.4**. The only downside of this approach is that it may require the fabrication of a few panels with smaller widths to accommodate the skew without the end panels becoming too narrow at one end. Both options should include support of the panel edges at the abutments.
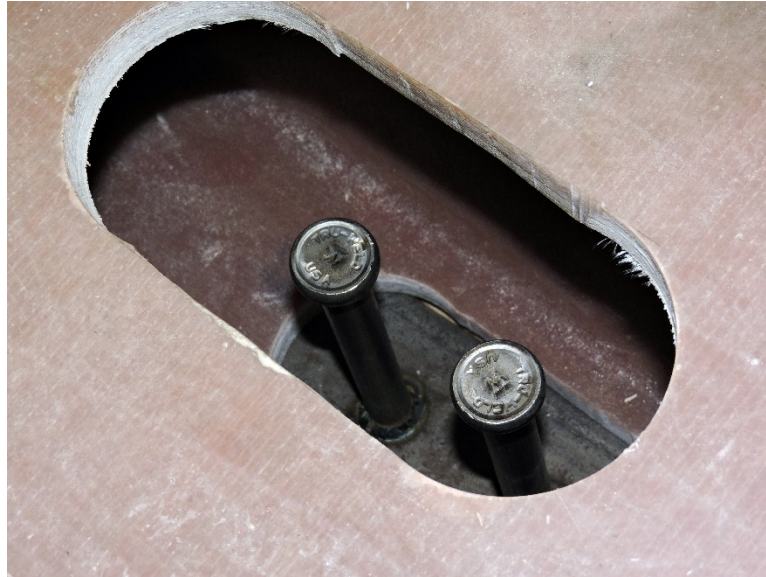

Figure 8.1: Headed Shear Stud Pocket

8.3. DECK DRAINAGE

Penetrations in the FRP deck to accommodate drain lines are easily accommodated with the layup process used to construct the panels (Section 2). Localized reinforcement may be required depending on the size and location of the penetrations. Inserts can also be easily accommodated during the fabrication process to facilitate installation of the drain lines.

8.4. COSTS

Previous installed FRP deck costs have ranged from $65 to $95 per square foot (Bakis et al., 2012). The research team estimates a reduced installed cost of approximately $45 per square foot for the prototype FRP deck panels. Although a significant improvement over previous FRP deck systems, the cost is still noticeably above the installed $30 per square foot cost using conventional deck construction materials. However, given the closer initial costs and the much lower life-cycle costs for an FRP deck system, state DOTs may consider this a viable initial or deck replacement option.

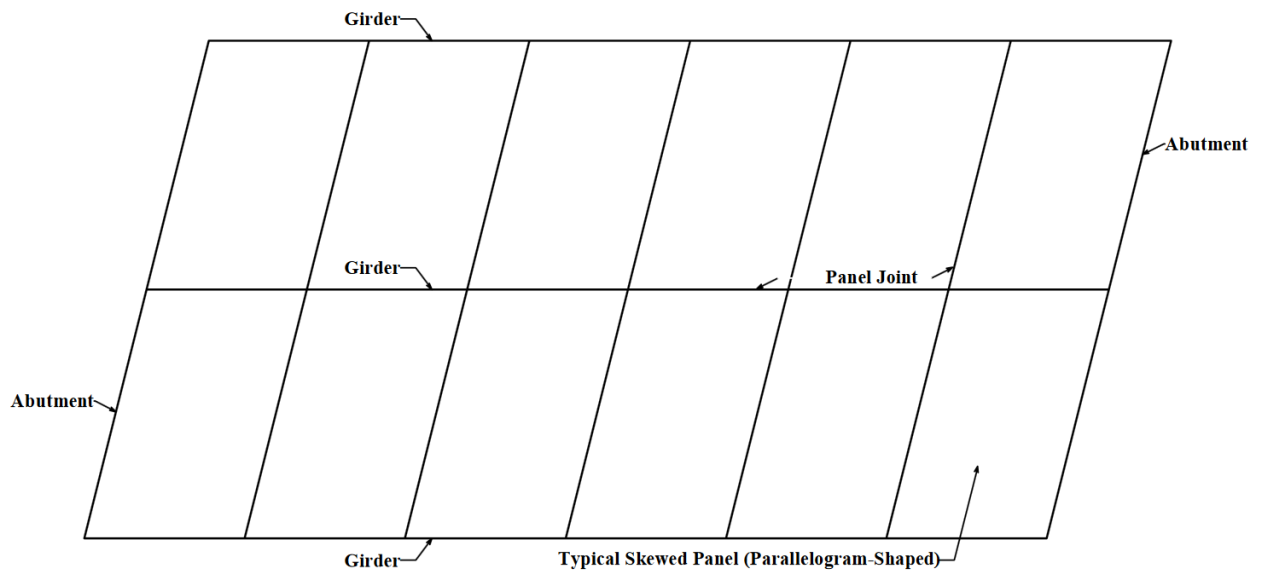**Figure 8.2: Headed Shear Stud Pocket After Grouting**

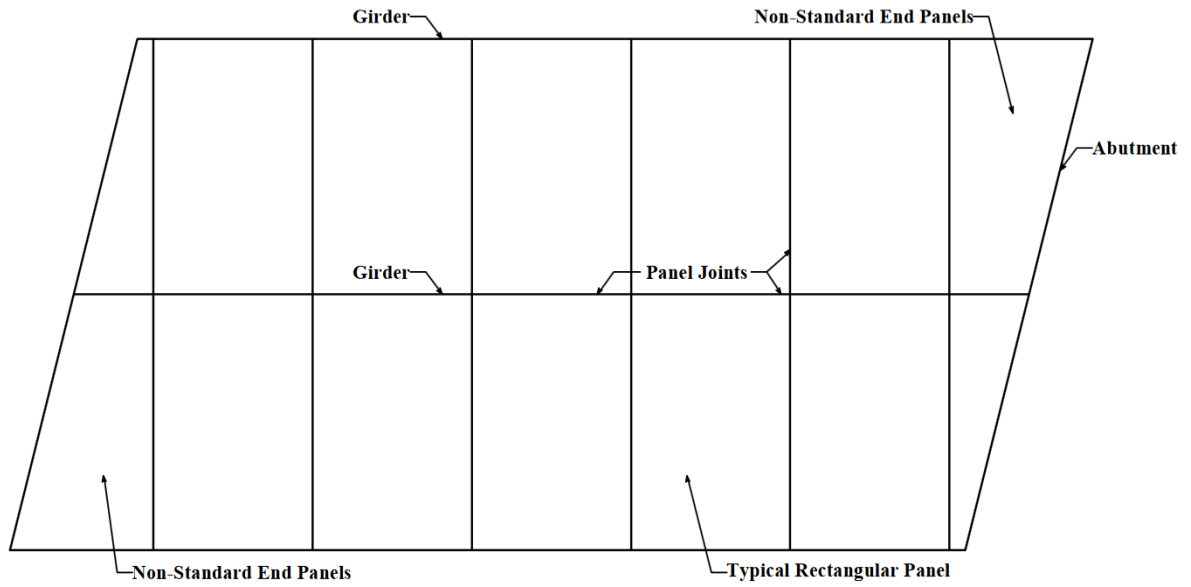**Figure 8.3: Skewed Bridge Option 1 – Skewed Panels**

Figure 8.4: Skewed Bridge Option 2 – Rectangular Panels with Non-Standard End Panels

REFERENCES

Alampalli, S., O'Connor, J., and Yannotti, A.P. (2000). *Design, Fabrication, Construction, and Testing of an FRP Superstructure*, Special Report 134, Transportation Research and Development Bureau, New York State Department of Transportation, Albany, NY.

American Association of State Highway Transportation Officials (AASHTO). (2013). *AASHTO LRFD Bridge Design Specifications*, 6th Edition, 2013 Interim Revisions, Washington, D.C.

Cassity, P., Richards, D., and Gillespie, J. (2002). "Compositely Acting FRP Deck and Girder System," *Structural Engineering International*, 12(2):71-75.

El-Aasar. (2015). *The Development of Crashworthy Rails for Fiber Reinforced Polymer Honeycomb Bridge Deck System*, Report No. FHWA-KS-15-03, Kansas Department of Transportation, Topeka, KS.

Federal Highway Administration (FHWA). (2013). *Composite Bridge Decking*, Final Report, Publication No. FHWA-HIF-13-029, Washington, D.C.

Link, C.T. (2003). "Development of Panel-to-Panel Connections for use with a Pultruded Fiber Reinforced Polymer Bridge Deck System," M.E. Report, Virginia Polytechnic Institute and State University, Blacksburg, VA.

Liu, Z. (2007). "Testing and Analysis of a Fiber-Reinforced Polymer (FRP) Bridge Deck," Ph.D. Dissertation, Virginia Polytechnic Institute and State University, Blacksburg, VA.

National Cooperative Highway Research Program (NCHRP). (2002). *Development of a Generic Connector System for Attaching Conventional Bridge Rails to FRP Composite Bridge Decks*, Final Report, NCHRP-IDEA Project 80, Transportation Research Board, Washington, D.C.

Naval Facilities Engineering Command (NAVFAC). (2005). "Fiber-Reinforced Polymer Composites in Bridges: A State-of-the-Art Report," Technical Memorandum TM-2384-SHR, Port Hueneme, CA.

Rocca, S.V. and Nanni, A. (2005). "Mechanical Characterization of Sandwich Structure Comprised of Glass Fiber Reinforced Core: Part 1," *Proceedings of Composites in Construction: Third International Conference*, Lyon, France, pp. 11-13.

Zetterberg, T., Astrom, B.T., Backlund, J., and Burman, M. (2001). "On Design of Joints between Composite Profiles for Bridge Deck Applications," *Composite Structures*, 51(1):83-91.